ATLAS-ASSISTED SEGMENTATION OF HIPPOCAMPUS

PHAM DUC MINH

(M.Sc, NUS)

A THESIS SUBMITTED

FOR THE DEGREE OF MASTER OF SCIENCE

SCHOOL OF COMPUTING

NATIONAL UNIVERSITY OF SINGAPORE

2005

Acknowledgement

First and foremost, I am deeply indebted to my supervisors, Dr. Nowinski Wieslaw, Dr. K.N Bhanu Prakash , and Associate Professor Leow Wee Kheng, for their precious guidance, direction insight, heuristic instructions, continuous support, and encouragement throughout my thesis. I am also grateful to Dr. Aamer Aziz, and Dr. Mikalai Ivanou, for their help and guidance throughout the master project.

I would like to thank my close friend Pham Nam Trung for his support during my study in Singapore as well as his discussion about the project.

I also thank to my friends Pham Viet Thang, Dinh Trung Hoang, Tran Quoc Long, Ho Dac Phuong, Ta Minh Chien because of their support for my study and living in Singapore.

Thanks to Mr. Zuo Wei, Mr Li Yang for their helpful discussions and comments on the project.

Finally, I am grateful to the Biomedical Imaging Lab, A*STAR, and National University of Singapore for providing me the chance to study in Singapore.

Table of Content

List of Figures

List of Symbols

MRI: Magnetic Resonance Imaging

CT: Computerised Tomography

GVF: Gradient Vector Flow

ROI: Region of interest

FP: False positive

FN: False negative

Abstract

The hippocampus is a small gray matter structure that is adjacent to other gray matter structures e.g amygdala, parahippocampus gyrus. The hippocampus has no clearly distinguishable boundaries along significant portion of its surface . That is why segmentation of hippocampus from its neighbors is still a challenge of medical image processing. I propose an atlas-assisted method to segment the hippocampus in brain MR neuroimages. The method is implemented in two steps: global and local. In the global step, the initial location of the hippocampus is determined by a brain atlas registered with the scan. For registration, we use the modified Talairach transformation based on the midsagittal plane, anterior and posterior commissures, and the extents of the brain. In the local step, this coarse segmentation is refined locally of applying active contours with anatomical knowledge constraints.

Chapter 1

Introduction and Motivation

The rapid development and proliferation of medical imaging technologies is revolutionizing medicine. Medical imaging allows scientists and physicians to glean potentially life-saving information by peering noninvasively into the human body. The role of medical imaging has expanded beyond the simple visualization and inspection of anatomic structures. It has become a tool for surgical planning and simulation, intra-operative navigation, radiotherapy planning, and for tracking the progress of disease. For example, ascertaining the detailed shape and organization of anatomic structures enables a surgeon preoperatively to plan an optimal approach to some target structure. In radiotherapy, medical imaging allows the delivery of a necrotic dose of radiation to a tumor with minimal collateral damage to healthy tissue.

With medical imaging playing an increasingly prominent role in the diagnosis and treatment of disease, the medical image analysis community has become preoccupied with the challenging problem of extracting, with the assistance of computers, clinically useful information about anatomic structures imaged through CT (Computed Tomography), MR (Magnetic Resonance), PET (Positron Emission Tomography), and other modalities. Although modern imaging devices

provide exceptional views of internal anatomy, the use of computers to quantify and analyze the embedded structures with accuracy and efficiency is limited. Accurate, repeatable, quantitative data must be efficiently extracted in order to support the spectrum of biomedical investigations and clinical activities from diagnosis to radiotherapy to surgery.

Nowadays, medical image applications have been developed rapidly. In most applications that use medical image data, segmentation is an important step. For example, segmentation is a prerequisite for quantification of morphological disease manifestation and for radiation treatment planning. The results of segmentation can be used to construct anatomical models. The brain atlases are used in stereotactic neurosurgery, neuroradiology and human brain mapping. The data from segmentation also can be used for visualization of individual objects.

In our project, we focus on the *segmentation of the human hippocampus*. The hippocampus is a part of the brain located inside the temporal lobe (humans have two hippocampi, one in each side of the brain). It forms a part of the limbic system and plays a major role in *memory* and *navigation*. The limbic system is a group of brain structures that are involved in various *emotions* such as aggression, fear, pleasure and also in the formation of memory. The location and shapes of structures in limbic system is in *Fig.* 1 and *Fig*.2 (from Internet).

► **Location of Major Limbic System Structures**

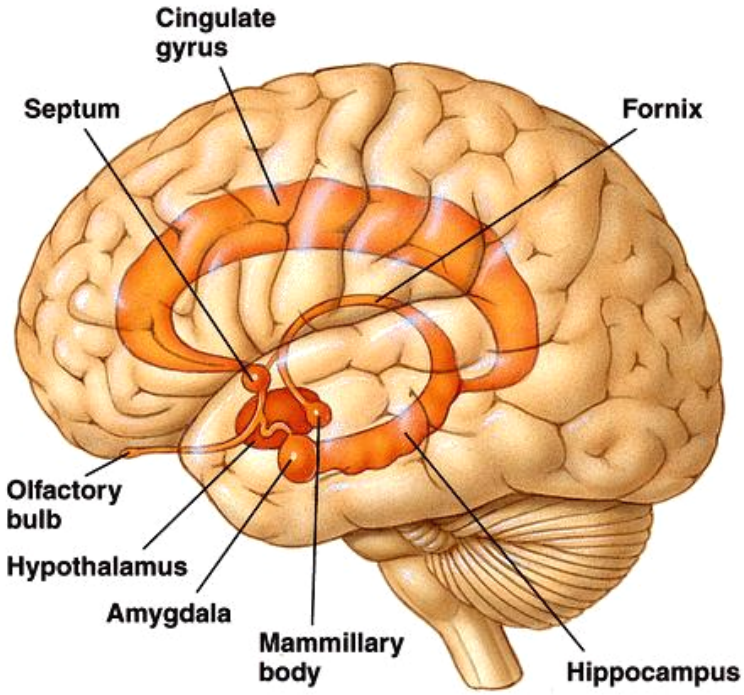

Figure 1 Location of Major Limbic System Structures

► **Major Components of the Limbic System**

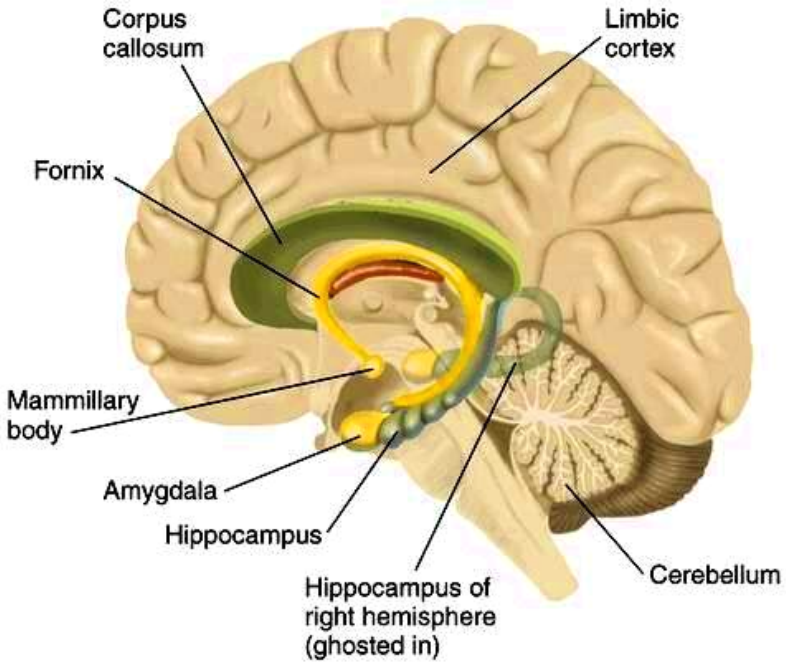

Figure 2 Major components of the Limbic System

The hippocampus is one of the first region to be affected by Alzheimer's disease causing memory problems and disorientation as the first symptom. Damage to the hippocampus can also result from oxygen starvation (anoxia) and encephalitis. The hippocampus has an essential role in the formation of new memories about personally experienced events. Some evidence implicates the hippocampus for storing and processing spatial information. Abnormalities of hippocampal anatomy occur in schizophrenia and support current hypothese that schizophrenia involves a disturbance of hippocampal-prefrontal connections. Therefore, the study of hippocampus is very important and necessary for clinical analysis. From the segmentation of the hippocampus, the doctor can diagnose the nature of disease.

The hippocampus is a small gray matter structure that is adjacent to some other gray matter structures (e.g amygdala, parahippocampal gyrus). The hippocampus has relatively low contrast and no distinguishable boundaries along significant portion of its surface. That is why segmentation of hippocampus from its neighbors is still a challenge of medical image processing.

So far, there has been some research about segmentation of hippocampus. However, atlas-assisted segmentation of hippocampus has not been studied. The atlas will speed up the segmentation and facilitate acceptance in clinical practice. In our project, we use the atlas as an assistant to segment the hippocampus from MR images.

Chapter 2

Background

2.1 Brain atlases

Before the prevalence of Information Technology, a number of excellent *printed atlases* had already been available, such as, DUVERNOY (1988), NETTER (1991). In addition, several stereotactic brain atlases have also been constructed: TALAIRACH and TOURNOUX (1988, 1993). These atlases are usually based on a single, at best several, specimen. They only provide some very general and non-specific information and are used as a reference model. Furthermore, because they are printed on paper, a major limitation of these atlases is the difficulty in mapping the printed atlas plates into an individual brain [Nowinski, 2002].

In order to overcome the disadvantage of the printed atlases, *electronic atlases* were developed. Electronic atlas is not just a simple electronic transformation of the printed atlas. It is a rather complex system consisting of 3 major components (as shown in *Fig.* 3) [Nowinski, 2002]. Brain model is the graphic databases containing contours, surfaces, polygonal or volumetric models. Textural database

is a list of the anatomy structures with their anatomical name and description. Tools provide some operations such as registration, labeling, presentation and mensuration.

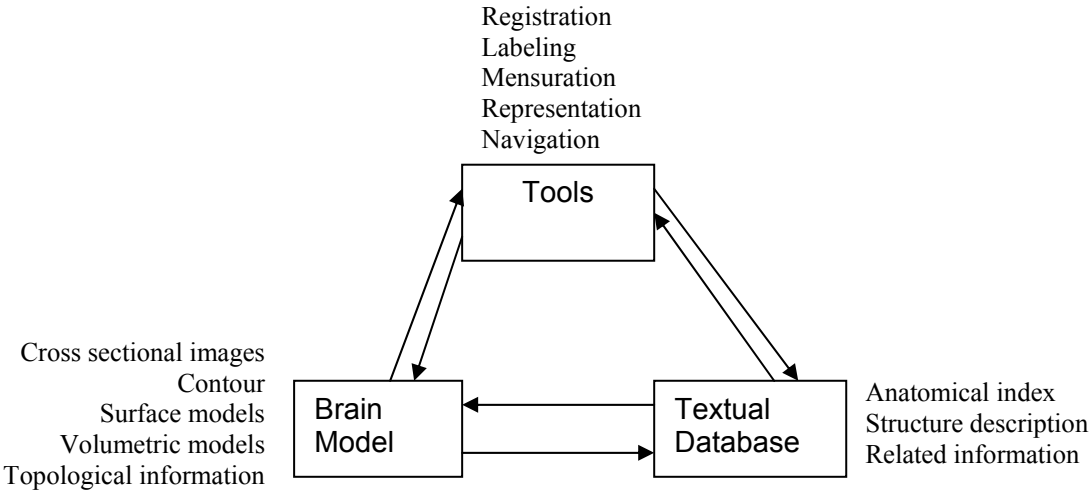

Figure 3 [Nowinski, 2002]

These deformable electronic atlases overcome some limitations of the printed atlas and even give new possible applications. They offer many features not available in printed atlas, such as interactive labeling of scans, selectable visualization in 2D or 3D, defining the regions of interest (ROI), and integration information from multiple sources. Combining with the widely accepted stereotactic printed atlas with the new features provided by the electronic atlases, many printed atlases have been converted into electronic form. Among them, Cerefy electronic brain atlas database [Nowinski 1997a; Nowinski 2001a] contains electronic version of several printed brain atlases published by Thieme (Schaltenbrand and Wahren 1977; Talairach and Tournoux 1988; Ono et al 1990; Talairach and Tournoux 1993). This databse has been used for many clinical and educational applications [Nowinski et al. 2000, 2001b, 2003a, 2003b].

2.2 Medical Image Segmentation

2.2.1 Terminology

In this section we define some terminologies that are used in our project.

Definitions

An image may be defined as a two-dimensional function, *f(x, y)*, or a three-dimensional function, *f(x, y, z)*, where *x* and *y* and *z* are spatial coordinates, and the amplitude of *f* is called the intensity or gray level of the images at that point. When *x*, *y*, *z* and amplitude values of *f* are all finite, discrete quantities, we call the image a digital image. Image intensities are measurements that can be radiation absorption in X-ray imaging, acoustic pressure in ultrasound, or RF (Radio Frequency) signal amplitude in MRI. If a single measurement is made at each location in the image, then the image is called a scalar image. If more than one measurement is made (eg. Dual-echo MRI), the image is called a vector or multi-channel image.

The term image segmentation refers to the partition of an image into a set of regions that cover it. These nonoverlapping, constituent regions which are homogeneous with respect to some characteristics such as intensity or texture. If the domain of the image is given by *I*, then the segmentation problem is to determine the sets $S_k \subset I$ whose union is the entire image *I*. These sets must satisfy

$$I = \bigcup_{k=1}^{K} S_k$$

where $S_k \cap S_j = \phi$ for $k \neq j$, and each S_k is connected.

Labeling is the process of assigning a meaningful designation to each region or class and can be performed separately from segmentation. It maps the numerical index k of the set S_k to the anatomical designation. In medical imaging, the labels are visual and can be determined by a physician or technician.

Dimensionality

Dimensionality refers whether a segmentation method operates on a 2-D image or a 3-D image. Methods that are based on image intensity are independent on the image dimensionality. Some methods such as deformable models, Markov random fields, region growing incorporate spatial information. Therefore, these methods operate differently on 2-D and 3-D images. A 2-D method can be used for 3-D images by implementing slice by slice of 3-D images. This method has some advantages such as ease of implementation, lower computational complexity, and less memory requirements.

Soft segmentation and partial volume effects

Segmentations that allow regions or classes to overlap are called soft segmentation. Soft segmentation is important in medical imaging because of partial volume effects, where multiple tissues contribute to a single pixel or voxel resulting in a blurring of intensity across boundaries (see *Fig.* 4).

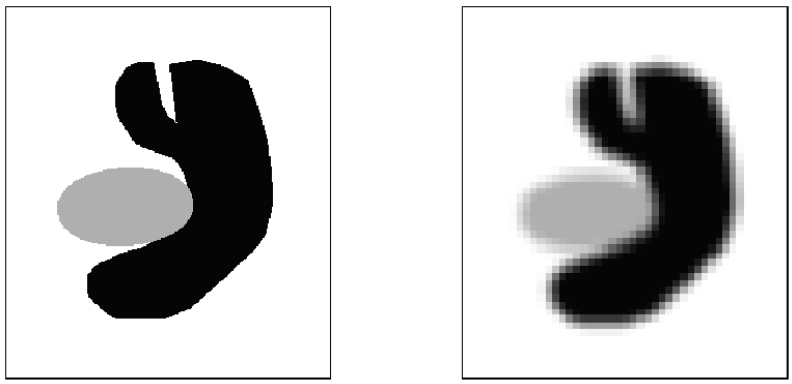

Figure 4 Illustration of the partial volume effect: a) Ideal image, b) acquired image [Dzung 1998].

A hard segmentation gives a decision whether a pixel is inside or outside the object. Soft segmentation retains more information from the original image by allowing for uncertain location of object boundaries.

Interaction

Interaction implies the interaction between the user and the implementation of the algorithm. The tradeoff between manual interaction and performance is an important consideration in any segmentation application. Segmentation methods can be classified into: manual, automatic and semi-automatic. A manual method with incorporated prior knowledge of an operator usually gives high accuracy. However, this method is laborious, time consuming and requires higher computational cost. Even automatic methods still require some interaction for specifying initial parameters that affect the segmentation performance.

Validation

After segmenting the object, we need validation experiments to determine sensitivity and specificity to make sure that our segmentation method is accurate. The straightforward approach is to compare the automated segmentations with manually obtained segmentations. The other approach is through the use of physical phantoms or computational phantoms.

2.2.2 Overview of Medical Image Segmentation Methods

In this section, we have a quick overview of some segmentation methods before going to some specified methods used in segmentation of hippocampus.

Thresholding

The thresholding approaches segment images by creating a binary partitioning of the image intensities. A thresholding procedure attempts to determine an intensity value, called the *threshold*, which separates the desired image into required segments. The segmentation is achieved by grouping all pixels with intensity greater than the threshold into one class, and all other pixels into another class. Thresholding is a simple effective means for obtaining a segmentation in images where different structures have contrasting intensities or other quantifiable features [Shiffan 2000].

The limitation of thresholding is that in its simplest form of only two classes cannot applied to multi-channel images. Moreover, thresholding does not take into

account the spatial characteristics of an image so it is independent of spatial configuration. Because of these issues, this method is sensitive to noise and intensity inhomogeneties.

Region Growing

Region growing is a technique for extracting a region of the image that is connected based on some predefined criteria. This criteria can be based on the intensity information or edges. At first, the algorithm needs a seed point and after that the region is grown from the seed point. A neighbor of the region can be added if it satisfies some criteria. In its simplest form, region growing requires a seed point that is manually selected by an operator, and extracts all pixel connected to the initial seed with the same intensity value or the same range.

Like thresholding, region growing is not usually used alone. The primary disadvantage is that the algorithm requires a seed point manually planted. Therefore, for each region that needs to be extracted, a seed needs to be planted. Region growing can also be sensitive to noise, causing extracted regions to have holes or even become connected. The result of region growing may be unsatisfactory when complicated structures are to be segmented. Seed can also be selected automatically. Defining the parameters of region growing may be difficult.

Classifier

Classifier methods are pattern recognition techniques that partition a feature space derived from the image. Classifier methods are supervised method because they use training data that are manually segmented and labeled and then used as references for automatically segmenting new data. There are a number of ways in which training data can be applied in classifiers methods. A simple classifier is the nearest-neighbor classifier, where each pixel or voxel is classified in the same class as the training datum with the closest intensity. The k-nearest-neighbor (kNN) classifier is a generalization of this approach, where the pixel is classified according to the majority vote of the k closest training data. The kNN classifier is considered a nonparametric classifier since it makes no underlying assumption about the statistical structure of the data. Another nonparametric classifier is Parzen window, where the classification is made according to the majority vote within a predefined window of the feature space centered at the labeled pixel intensity. A commonly-used parametric classifier is the maximum likelihood or Bayes classifier. It assumes that the pixel intensities are independent samples from a mixture of probability distribution, usually Gaussian.

Standard classifiers require that the structures to be segmented possess distinct quantifiable features. Because training data can be labeled, classifiers can transfer these labels to new data as long as the feature space sufficiently distinguishes each label as well. Being non-iterative, they are relatively computationally efficient. Unlike thresholding methods, classifiers can be applied to multi-channel images.

A disadvantage of classifiers is that they generally do not perform any spatial modeling. This weakness has been addressed in recent work to segmenting images that are corrupted by intensity inhomogeneities. Another disadvantage is the requirement of manual interaction for obtaining training data. Training sets can be acquired for each image that requires segmenting, but this can be time consuming and laborious [Karayiannis 1999], [Dzung 1999], [Barra 2001].

Clustering

Clustering algorithms essentially perform the same function as classifier methods without the use of training data. Therefore, they are termed unsupervised methods. Without the training data, clustering methods train themselves by using the available data.

Although clustering algorithms do not require training data, they do require an initial segmentation (or equivalently, initial parameters). Like classifier methods, clustering algorithms do not directly incorporate spatial modeling. Thus, the result is sensitive to noise and intensity inhomogeneities. This lack of spatial modeling, however, can provide significant advantages for fast computation.

Artificial Neural Network

Artificial neural networks (ANNs) are massively parallel networks of processing elements or nodes that simulate biological learning. Each node in ANN performs

elementary computations. Learning is archieved by the adaptation of the weight of the connection assigned to each node.

ANNs represent a paradigm for machine learning and can be used in a variety of ways for image segmentation. The most widely applied use in medical imaging is as a classifier, where the weights are determined using training data, and the ANN is then used to segment new data [Reyes-Aldasoro 1999].

Morphology-based

Geraud et al [Geraud 1998] introduced a method that relies mainly on morphological information. The method is basically based on the mean and variation gray value of the structures. Although the accuracy of the segmentation is not stable in some structures, this methods can be improved by combining with more statistical methods (Markov Random Fields for instance) or be the initialization for other model-based recognition method.

A grey-level morphology-based is proposed by Hult [Hult 2003]. This approach is similar to other histogram-based methods. The grey-level morphology is used with binary morphology.

Deformable Models

Deformable models are physically motivated, model-based techniques for delineating region boundary using closed parametric curves or surfaces that deform under the influence of internal and external forces. Among model-based

techniques, deformable models offer an approach that combines geometry, physics, and approximation theory. Geometry represents the shape of object and physics imposes constraints on how the shape may vary over space and time. Optimal approximation provides the solution how to fit the models to measured data.

The potency of deformable models stems from their ability to segment, match, and track images of anatomic structures by exploiting (bottom-up) constraints derived from the image data together with (top-down) a priori knowledge about the location, size, and shape of these structures. The important capability of deformable models is that they can accommodate the often significant variability of biological structures over time and across different individuals.

The deformable model that has attracted the most attention to date is popularly known as “snakes” [Kass 1988]. Snakes or “deformable contour models” represent a special case of the general multidimensional deformable model theory. We will review their simple formulation in the remainder of this section in order to illustrate the basic mathematical machinery that is present in many deformable models.

Energy-Minimizing Deformable Models

The active contour model, or snake, is defined as an energy minimizing spline – the snake's energy depends on its shape and location within the image [Kass 1988]. The snake model represents a contour **x** as

$$\boldsymbol{x} = \boldsymbol{x}(s) = (x(s), y(s)) \qquad 0 \le s \le 1$$

and x and y are the coordinates of a contour point.

The snake is deformed under the influence of three forces:

- Internal forces (E_{int}): constraining the stretching and banding of the snake.
- Image forces (E_{image}): forces are derived from the image data over which the snake lies.
- External forces (E_{con}): external constraints imposed either by a user or some other higher level process which may force the snake toward or away from particular features.

The total energy of the snake is

$$E_{snake} = \int_0^1 [E_{\text{int}}(x(s))] + E_{image}(x(s)) + E_{con}(x(s))]ds$$

The local minimum of this energy corresponds to desired image properties.

The deformable model combines three types of information. First, it employs information about the geometric properties of the object boundary, from a local and relatively finer scale to a more global and relatively coarser scale. Second, the model includes a statistical characterization of normal shape variation across individuals, serving as prior knowledge to the algorithm. Third, the algorithm utilizes a number of manually defined boundary points, which can help guide the model deformation to the appropriate boundaries, wherever these boundaries are weak or not clearly defined in MR images [Shen 2001b].

The disadvantage is that deformable models require manual interaction to place an initial model and choose appropriate parameters.

Atlas-guided approaches

Atlas-guided approaches are a powerful tool medical image segmentation when a standard atlas or template is available. At first, the atlas is generated by compiling information on the anatomy of image data. After that, this atlas is used as a reference to segment new images. Conceptually, the atlas-guided approaches are quite similar to classifiers. However, they are implemented in the spatial domain of the image rather that the feature space.

The standard atlas-guided approach treats segmentation as a registration problem. It first finds a one-to-one transformation that maps a pre-segmented atlas image to target image that requires segmenting. This process is often referred to as atlas warping.

Atlas-guided approaches have been applied mainly in brain imaging. An advantage of atlas-guided approaches is that labels are transferred along with the segmentation [Rohlfing 2004].

2.3 Active Contours

Snakes, or active contours, are curves defined within an image domain that can move under the influence of internal forces coming from within the curve itself and external forces computed from the image data. The internal and external

forces are defined so that the snake will conform to an object boundary or other desired features within an image. Active contours synthesize parametric curves within an image domain and allow them to move toward desired features, usually edges.

There are two key problems with active contour algorithms. First, in general, the initial contour must be close to the true boundary. Otherwise, it will converge to the wrong result. The second problem is that active contours have difficulties progressing into boundary concavities.

Traditional snake

A traditional snake is a curve $\mathbf{v}(s) = [x(s), y(s)]$, $s \in [0, 1]$. It has the energy function

$$E = \int_0^1 \frac{1}{2}\left[\alpha|v'(s)|^2 + \beta|v''(s)|^2\right] + E_{ext}(v(s))ds$$

where α and β are weighting parameters that control the snake's tension and rigidity, respectively, and $v'(s)$ and $v''(s)$ denote the first and second derivatives of $v(s)$ with respect to s.

The external energy function E_{ext} is derived from the image so that it takes smaller values at the boundaries. Given a gray-level image $I(x, y)$, the external energy is defined as

$$E_{ext}^{(1)}(x, y) = -|\nabla I(x, y)|^2$$

or

$$E_{ext}^{(2)}(x,y) = -\left|\nabla[G_\sigma(x,y) * I(x,y)]\right|^2$$

where $G_\sigma(x,y)$ is a two-dimensional Gaussian function with standard derivation σ and ∇ is the gradient operator. Larger σ's will cause the boundaries to become more blurry.

A snake that minimizes *E* must satisfy the Euler equation

$$(\alpha v'(s))' - (\beta v''(s))'' - \nabla E_{ext} = 0$$

A numerical solution to this equation can be found by discretizing the equation and solving the discrete system iteratively [Kass 1988].

Behavior of traditional snake

The illustration of behavior of traditional snake is in *Fig.* 5.

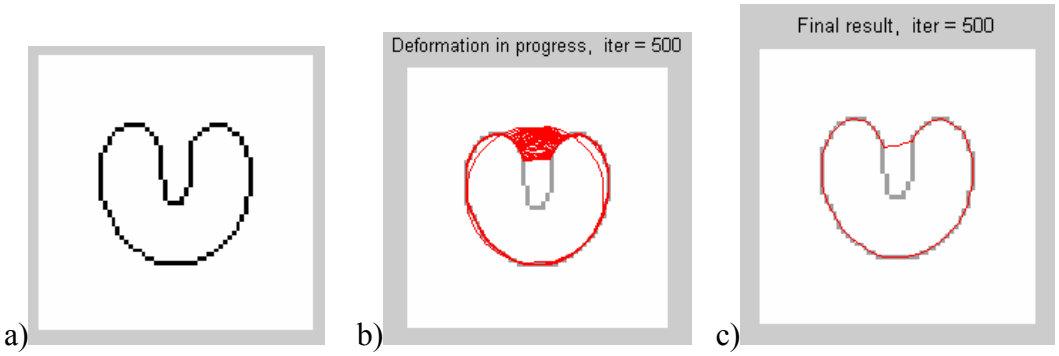

a) b) c)

a) The U-shape test object. b)The progress of deformation during running. c)The final result after iteration 500.

Figure 5 Running of traditional snake contour algorithm.

Gradient Vector Flow Snake

The traditional snake has two main shortcomings:

- It does not converge well to concave features
- Its performance is sensitive to initial guess of snake point positions

Gradient Vector Flow (GVF) overcomes these shortcomings. It is based on diffusion of gradient vectors of edge map.

It is solved numerically by discretization and iteration, in identical fashion to the traditional snake.

Defining *f(x, y)* as *edge map* derived from the image *I(x, y)*. Three properties of edge maps are important. First, the gradient of an edge map ∇f is normal to the edges at the edges. Second, these gradients have large magnitudes only in the immediate vicinity of the edges. Third, in the homogeneous regions, *I(x, y)* is nearly constant, ∇f is nearly zero. The gradient vector flow field *g(x, y)* = [*u(x, y), v(x, y)*] is the vector field that minimizes the energy functional

$$\varepsilon = \int\int \mu(u_x^2 + u_y^2 + v_x^2 + v_y^2) + \left|\nabla f\right|^2 \left|g - \nabla E\right|^2 dxdy$$

When ∇f is small, the energy is dominated by the sum of the squares of the partial derivatives of the vector field, yielding a slowly varying field. When ∇f is large, the second term dominates the integrand, and is minimized by setting $\mathbf{v} = \nabla f$. This produces the desired effect of keeping **v** nearly equal to the gradients of the edge map when it is large, but forcing the field to be slowly-varying in homogeneous regions. The parameter μ is regularization parameter governing the tradeoff between the first term and the second term in the integrand. This parameter should be set according to the amount of noise present in the image (more noise, increase μ).

The GVF can be found by solving the following Euler equations

$$\mu\nabla^2 u - (u - f_x)(f_x^2 + f_y^2) = 0$$

$$\mu\nabla^2 v - (v - f_y)(f_x^2 + f_y^2) = 0$$

where ∇^2 is the Laplacian operator. In a homogeneous region [where *I(x, y)* is constant], the second term in each equation is zero because the gradient of *f(x, y)* is zero. Within such a region, u and v are each determined by the Laplace's equation, and the resulting GVF field is interpolated from region's boundary, reflecting a kind of competition among the boundary vectors. This explains why GVF yields vectors that point into boundary concativites.

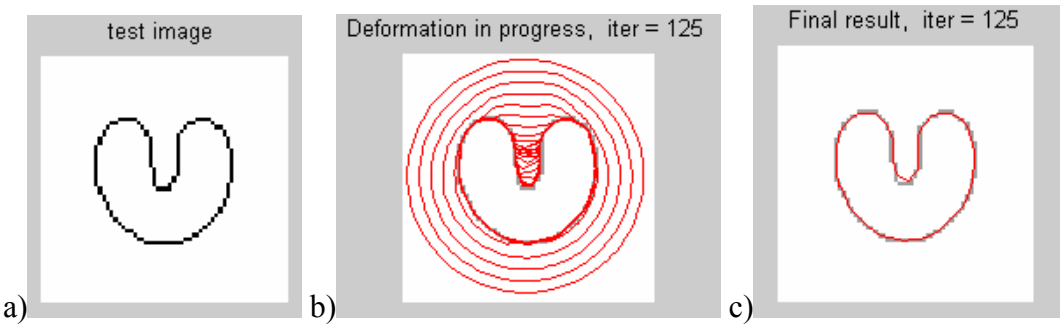

a) The U-shape test object. b) The progress deformation during running of GVF algorithm. c) The final result with iteration 125 times.

Figure 6 Results of GVF contour algorithm.

Chapter 3

State Of The Art Review Of Segmentation of Hippocampus

In this chapter, we do a literature review of previous and current research that is relevant to the project. The literature review mostly refers to segmentation and shape analysis of hippocampus.

In the following parts, we will analyze some outstanding research on segmentation and modeling of the hippocampus. Methods for segmenting hippocampus can be classified into: manual, automatic and semi-automatic.

3.1 Manual segmentation methods of hippocampus

In [Csernansky 1998], Csernansky et al used transformations of neuroanatomical template containing expert-derived information about the boundaries of the left and right hippocampus to compare subjects with schizophrenia and healthy control subjects. An analysis of hippocampal shape as well as volume was carried out. To highlight the specificity of the shape comparison findings, hippocampal shape deformations found in the schizophrenia subjects were compared with patterns of normal hippocampal shape variability and to the hippocampal shape deformation found in a single subject with mild dementia of the Alzheimer type. The landmarks in the MR scan placed were based on the properties of anterior and posterior commissures in the midsagittal plane. The template was produced from

healthy controls manually by the consensus of three experts. This method had a remarkable accuracy in segmenting the hippocampus at a high computational cost.

In [Joshi 1997], for segmentation of hippocampus, the authors represent the typical global structures via the construction of templates. To represent the structures' variability, they define a probabilistic diffeomorphic transformation to apply to the templates. The transformations are defined by diffeomorphisms $h : \Omega \leftrightarrow \Omega$ of the coordinate system of the template defined as Ω. The dimension of the transformation,

$$h : x = (x_1, x_2, x_3) \in \Omega \mapsto h(x) = (h^1(x_1), h^2(x_2), h^2(x_3)) \in \Omega$$

is roughly equivalent to the number of voxels in the volume, thereby accommodating a variation in anatomy. A coarse-to-fine procedure is generated for generating the volume maps from the template to the target. The first step in the procedure is based on operator provided manifold information, the information corresponding to easily identifiable points, lines, surfaces. The second step is to solve the registration problem using the full volume data. The experiments and results presented in this paper are limited because the sample size studied consisted of only 10 pairs of schizophrenics and controls.

3.2 Semi-automatic segmentation methods of hippocampus

Automatic methods did not combine prior knowledge of hippocampal location, anatomic boundaries and shape. Some more realistic semi-automatic methods have been proposed to combine automatic techniques with prior knowledge

[Ashton 1997], [Shen 2001b] [Ghanei 1998]. Ashton et al [Ashton 1997] proposed an algorithm that uses elements of both deformable model and region growing techniques and incorporates a prior operator knowledge of hippocampal location and shape. A new 3D discrete dynamic model was used to segment hippocampus from brain MRI [Ghanei 1998]. The geometry of model deforms by internal forces (based on local geometry of the model and local curvature of the surface) and external forces (calculated from desired image features) after being generated by triangles patches. Another method using a deformable model for segmentation and quantification of the shape and size of the hippocampus was proposed in [Shen 2001b]. This model integrates geometric, statistical, and user-defined information.

Ashton et al. [Ashton 1997] introduced an algorithm that makes use of elements of both *deformable model* and *region growing* techniques and incorporates *a prior operator knowledge* of hippocampal location and shape. This method improves the snake-based techniques that do not incorporate any a *prior* model, the expected shape and size of the structure of interest. The algorithm begins with an initial simple shape model, composed of the superposition of multiple appropriately placed and shaped ovoids. This a prior modeling allows the algorithm to fill in area of the surface of the structure of interest which have no apparent boundary in the data. In addition, deformable model technique which incorporates some of the same goals as the region growing technique was proposed. At first, one or more seed voxels are planted. Each of seeds will, if left constrained, expand into an ovoid with a predetermined volume and preset ratios

between radii in the *x*, *y*, and *z* directions. Constraining forces are elastic surface tension, deviation from the expected surface normal, and resistance from surrounding tissue. The expansive force is provided by internal pressure, which is gradually increased until either the expected volume is reached or no further expansion is possible due to constraining tissue. The model proposed is an expanding bubble with a preset geometry. The expansive force at a given boundary is

$$F = p - (S + N + C)$$

where p is internal pressure, S is surface tension that is proportional to the total surface area of the model, N is deviation from expected surface normal, and C is the constraining force of the surrounding tissue.

Ghanei et al [Ghanei 1998] introduced a *geometric* structure used for deformation process. Basic geometry of the model surface is generated by triangle patches. The normal vector at each point that shows the local direction of the surface and is the base in computing internal forces is defined. The property of the normal vectors is that they point to the inside of the volume(see *Fig.* 9). Internal forces are elastic forces generated by the model geometry. The goal of internal forces is to smooth the surface and reduce its local curvature. A curvature definition at a point is defined by averaging on curvatures along different directions at that point. The external forces are computed from the volumetric data and show desired image features such as edges or lines. The resolution of the model is maintained by using a sampling procedure in each time step. This is done by adding vertices in the middle of large segments (See *Fig.* 7). An *initial shape* that is a closed surface is

produced from a stack of polygons drawn on parallel cross sections (See *Fig.* 8). This is a 3D deformable surface can be used for segmenting objects from 3D volume data in medical images. However, the model is dependent on parameter values and the initial polygon. The method does not incorporate information from multiple images normally acquired in MRI studies.

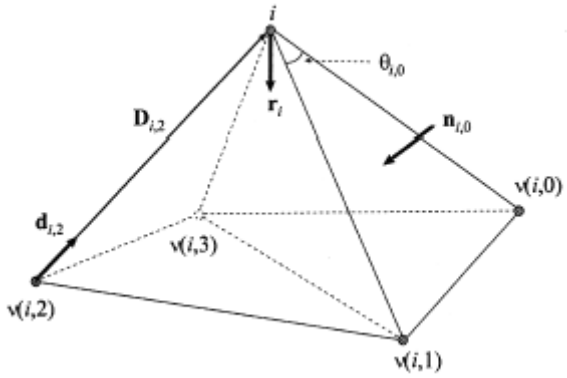

Figure 7 An example of the model structure with five vertices and five patches. The relative indices of four vertices relative to vertex i have been shown. Here, r_i is the unit radial vector of vertex i and $n_{i,0}$ is the unit normal vector perpendicular to the patch defined by vertices i, v(i, 0) and v(i, 1).

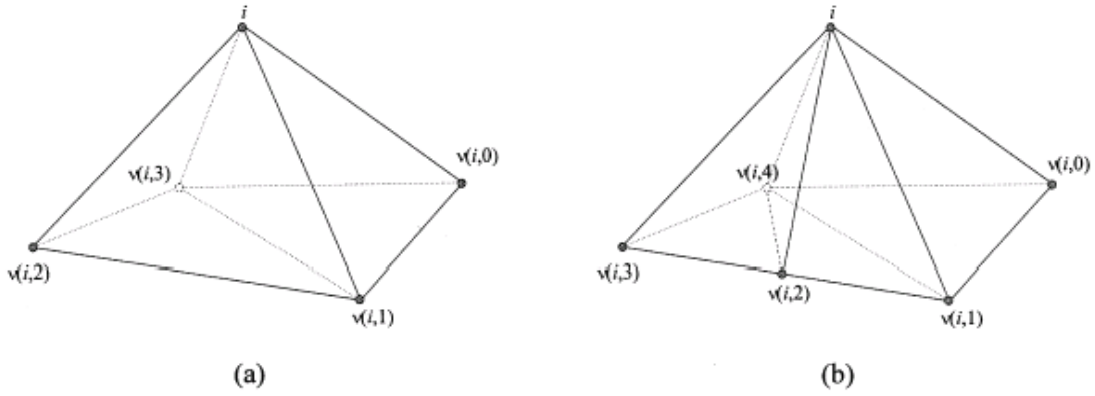

Figure 8 Resampling of the model to increase the resolution (a) Model before resampling. (b) Model after resampling. A vertex is added in the middle of the segment between v(i,1) and v(i,2).

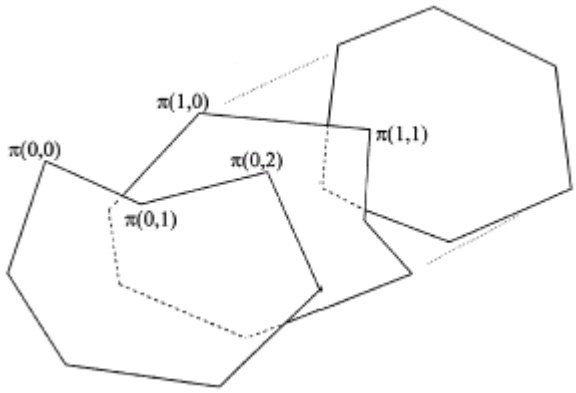

Figure 9 The initial shape is produced from a stack of polygons drawn by the user slice by slice. $\pi(l, k)$ is the k^{th} vertex of l^{th} polygon.

A deformable method using *attribute vectors* for measuring size and shape of the hippocampus was presented in [Shen 2001b]. The attribute vector is attached to each vertex of models, which reflects the model's geometric structure from a local to a global level. The energy function is composed of three terms.

$$E = \sum_{i=1}^{N} (E_i^{model} + \alpha_i E_i^{data}) + \sum_{j=1}^{L} \beta_j E_j^{landmark}$$

where N is the number of the vertices in the hippocampal model and L is the number of landmarks placed on the boundaries of the hippocampi. α_i and β_j are the parameters to control the relative importance of each energy term. The first term favors shapes that have attribute vectors similar to the model. The second term demands that the deformable model adhere to edges extracted from the MR images. The third term demands that the reconstructed hippocampus pass through the landmarks that are defined manually. The initialization process is guided by the manually placed landmarks. Attribute vectors help establish anatomical

correspondences between the model and an individual hippocampus. These attribute vectors also help to train the model in the stage in which the normal range of shape variation is determined from a training set, without the need for manual definition of homologies, which could be impossible in 3D. With the help of the statistical prior, the deformable model stays within the range of shapes that "look like hippocampi" and can avoid following incorrect and noisy edges. The main shortcoming of this method is the need for manual definition of a number of points along the hippocampal boundary.

3.3 Automatic segmentation methods of hippocampus

Deformable models have been applied in some research in segmentation of hippocampus. These researches have been developed from the basic idea of deformable models as presented in the previous chapter. However, for each research, deformable model is applied differently.

An automatic *model-based* segmentation of objects from volumetric image data was proposed in [Klemen 1999]. The development closely follows the seminal work of Taylor and Cootes [Cootes 1994] on active shape models, but is based on a hierarchical parametric object description rather than a point distribution model. The segmentation system includes both the building of statistical models and the automatic segmentation of new image data sets via a restricted elastic deformation of shape models. Geometric models are derived from a sample set of image data which have been segmented by experts. The traning set is segmented by manual

processing. The parametric shape representation is SPHARM (spherical harmonics) (see *Fig.* 10). The reference coordinate system is the standard stereotactic coordinate system proposed by Talairach for global alignment of the head image data sets. Basic features used for alignment are the approximation of the interhemispheric fissure by a midsagittal plane and the definition of the anterior and posterior commisure (AC-PC) (see *Fig.* 11). The surfaces of these binary objects are converted into parametric surface representations, which are normalized to get an invariant object-centered coordinate system. The shape representation results in a continuous mapping function between similar objects. A key step in the shape description of a surface is its mapping to the parameter space, the sphere. Any point on the surface must map to exactly one point on the sphere and vice versa. The location on the sphere corresponding to a surface point defines the surface parameters of the point. Corresponding points on different object surfaces are found by calculating a canonical parametrization, rather than by interactive selection of labeled sets of 3-D points. After transformation to canonical coordinates, the object descriptors are related to the same system and can be directly compared. Principal Component Analysis (PCA) is applied for eigenmodes, mean shape and variation. Augmenting geometric models with information about the gray-level environment of the model significantly improves the robustness of the segmentation. The statistics of the image intensity along one-dimensional profiles, orthogonal to the object surface at a discrete set of sampling points are examined. This approach makes use of two shape representations which are used in a vice versa fashion, taking advantage of shape descriptors

holding a compact global object characterization and of a set of surface points giving access to local shape objects.

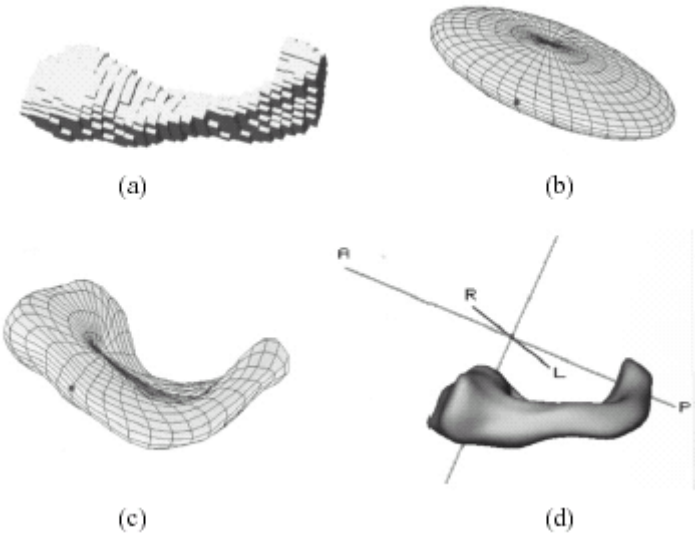

Figure 10 Model building. (a) Interactive segmentation of a left hippocampus. (b) Reconstruction from surface descriptor up to degree one. (c) Reconstruction up to degree ten. (d) Normalization of the shape pose in object space [Klemen 1999].

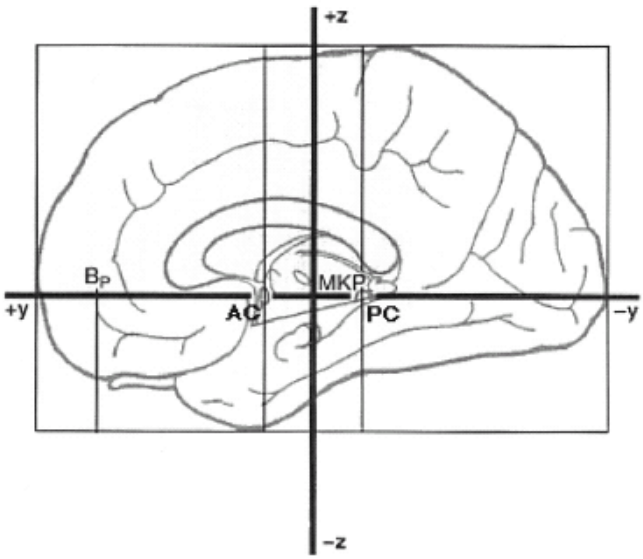

Figure 11 Stereotactic coordinate system used for object space normalization.

Crum et al presented an automated hippocampal segmentation by regional *fluid registration* [Crum 2001]. In this paper, the application of voxel-level three-dimensional registration to serial MRI is described. This fluid registration determines deformation fields modeling brain change, which are consistent with a model describing a viscous fluid. The segmentation algorithm consists of three steps. First, parameter choices for the fluid registration are investigated. Second, the technique is examined for repeatability and linearity. Third, this technique is used to measure simulated atrophy. The practical advantage of fluid registration over baseline manual segmentation for quantifying hippocampal change is that, given a baseline region, the match to a registered repeat region is deterministic.

Chapter 4

Proposed Algorithm for Segmentation of Hippocampus

In this section, we state the problems involved in segmentation of hippocampus and formulate the algorithm that we study in our research. Our research objective is to segment the hippocampus from the 3D MRI brain images.

The first problem is how to combine prior knowledge when segmenting the structure. One way is to change the prior knowledge into some parameters that are processed in the running of the algorithm (for example energy, force). Another way to use the prior knowledge is to identify the initially coarse position of the structure. This knowledge is derived from the anatomical knowledge because the relative position of structures is usually known. To identify initial coarse position is a challenging sub-problem to be solved in our research. We propose to combine the prior knowledge from the electronic atlas for segmentation.

We use the Cerefy Atlas of Brain Anatomy to assist segmentation. Two types of knowledge we derive from the electronic atlas are the position and the shape of hippocampus. The position and the shape are initial information put into the active contour. When the active contour runs, it will converge to the exact boundary of the structure.

The next problem is how to eliminate the user interaction of the algorithm. An ideal segmentation algorithm is the one that has automatic operation with high accuracy. So far, most automatic algorithms have only been applied on some simple objects and still need user interaction such as initializing parameters. In our research, we try to design a segmentation algorithm that is fully automatic and as accurate as possible. The results will be quantitatively compared with the ground truth determined by neuroanatomy experts.

We propose a two-steps knowledge-guided automatic segmentation algorithm. The first step is global segmentation where we identify the coarse position of hippocampus based on rotation, translation, and piece-wise linear scaling. The second step is the refinement of the hippocampus. The results obtained automatically by using our approach have to be quantitatively compared with the ground truth determined by neuroanatomy experts.

The algorithm was run with the data sets that have been provided by a local hospital and some hospitals from the US. To evaluate the algorithm, we used 10 data sets.

4.1 Global segmentation

The global segmentation step is mainly based on the Talairach transformation and the modified Talairach landmarks [Nowinski 2001a]. Talairach transformation is a piece-wise linear, landmark-based transformation. This transformation is based on the midsagittal plane (MSP), anterior commissure (AC), posterior commissure (PC), and the extent of the brain in anterior, posterior, dorsal, and ventral directions. The definition of AC, PC as well as how to find these points in MSP are explained in [Nowinski 2001a]. In addition, an algorithm for rapid and automatic extraction of the midsagittal plane of the human cerebrum from neuroimages is presented in [Hu 2003]. The detailed steps are diagrammed below (*Fig.* 12).

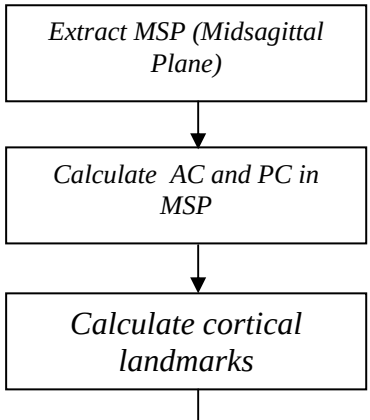

Figure 12 Flowchart for atlas-assisted global segmentation.

Cerefy Electronic Brain Atlas Database

The Cerefy electronic brain atlas database contains electronic versions of the printed brain atlases published by Thieme:

- *Co-planar Stereotactic Atlas of the Human Brain*

The Co-planar Stereotactic Atlas of the Human Brain [Talairach 1988] was constructed from a single brain specimen which had been sectioned and photographed sagittally, and coronal and axial sections were subsequently interpolated manually. To construct an electronic version, the printed plates were digitized with high resolution, and extensively preprocessed, enhanced and extended: (1) the original grids, rulers, and annotations were removed; (2) each atlas structure was assigned a unique color-coded representations, as opposed to a mixture of contour, color-coded, and texture representations in the printed atlas; (3)

the left thalamic nuclei, not available in the printed atlas on the axial and coronal plates, were outlined and color-coded; (4) the right hemisphere cortex for axial orientation was added by mirroring the left hemisphere cortex; (5) Brodmann's areas and gyri, which are labled but not segmented in the printed atlas, were constructed and color-code for axial orientation.

The electronic atlas database includes 3 directions: axial, coronal, sagittal. We segment hippocampus from the coronal direction.

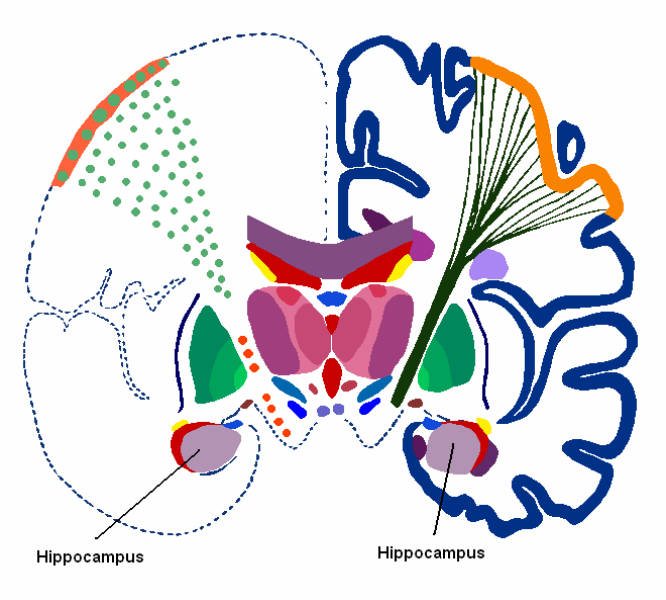

Figure 13 A coronal electronic atlas slice with the hippocampus labeled.

In the coronal direction, there are 38 slices, in which eights slices contain hippocampus. The size of the atlas slice is 660×600. An example of slice in coronal direction is in *Fig.* 13.

Talairach Transformation and Landmarks

The Talairach transformation [Talairach 1988] normalizes the brain piecewise linearly. It is based on the Talairach landmarks: two internal landmarks lying on the midsagittal plane and six external landmarks lying on the smallest bounding box encompassing the cortex. The Talairach landmarks are: AC – the anterior commisure is the intersection of the lines passing through the superior edge and the posterior edge of the anterior commissure; PC – the posterior commisure is the intersection of the lines passing through the inferior edge and the anterior edge of the posterior commissure; L(R) – most lateral point of the parietotemporal cortex for the left (right) hemisphere; A – most anterior point of the frontal cortex;; P – most posterior point of the occipital cortex; S – most superior (most dorsal) point of the parietal cortex; I – most inferior (most ventral) point of the temporal cortex.

The Talairach bounding box and the reference planes (i.e, the intercommissural plane, interhemispheric plane, and coronal planes passing through the AC and PC) divide the brain into 12 regions (*Fig*. 14)

The Talairach transformation normalizes brain images by warping the images within each of 12 regions linearly. In this way, the volumetric image of brain is warped in three dimensions piecewise linearly. The Talairach transformation can be used to warp one atlas against another, atlas against scan, or scan against atlas [Nowinski 2001a].

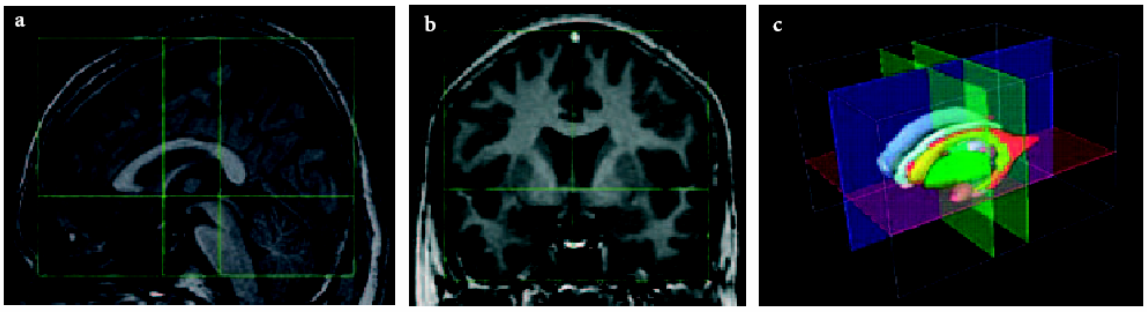

Figure 14 Talairach proportional grid system. **a** Sagittal orientation. **b** Coronal orientation. **c** In three dimensions [Nowinski 2002]

Modified Talairach Landmark

There are several problems associated with the original Talairach landmarks. First, not all of them are available in the original atlas. Second, locations of some landmarks in the atlas contradict their definitions. Third, the cortical landmarks are not defined in a constructive way. And fourth, the intercommisural landmarks are located beyond their own structures and, despite being defined constructively, their constructions are not easily feasible on a scanner console. To overcome these problems, Nowinski introduced a new, equivalent set of landmarks called the Talairach-Nowinski landmarks. The new landmarks are defined in a more constructive way than the original Talairach landmarks. In addition, they can be more easily identified automatically [Nowinski 2001a].

Two intercommissural lines are introduced: *central intercommissural line* and *tangential intercommissural line*. The central intercommissural line is passing the through the centres of the anterior commisure and the posterior commissure on the midsagittal (interhemishperic) plane. The tangential intercommissural line is tangential dorso-posteriorly to the anterior commissure and ventroanteriorily to the posterior commissure on the midsagittal plane.

The Talairach-Nowinski landmarks are defined as follows, see *Fig.* 15.

AC: The anterior commissure is a point within the intersection of the anterior commissure with the midsagittal (interhemispheric) plane. Three definitions of the AC landmarks are introduced:

central, where the AC landmark is the central point (the gravity center) of the anterior commissure

internal, where the AC landmark is the intersection of the central intercommissural line and the line passing through the posterior edge of the anterior commissure

PC: The posterior commissure is a point within the intersection of the posterior commissure with the midsagittal plane. Three definitions of the PC landmarks are introduced:

central, where the PC landmark is the central point (the gravity center) of the posterior commissure

internal, where the PC landmark is the intersection of the central intercommissural line and the line passing through the anterior edge of the posterior commissure

L: The point of intersection of three planes: the intercommissural (AC-PC axial) plane, the coronal plane through the PC, and the sagittal plane passing through the most lateral point of the parietotemporal cortex for the left hemisphere.

R: The point of intersection of three planes: the intercommissural plane, the coronal plane through the PC, and the sagittal plane passing through the most lateral point of the parietotemporal cortex for the right hemisphere.

A: The point of intersection of three planes: the intercommissural plane, the midsagittal plane, and the coronal plane passing through the most anterior point of the frontal cortex.

P: The point of intersection of three planes: the intercommissural plane, the midsagittal plane, and the coronal plane passing through the most posterior point of the occipital cortex.

S: The point of intersection of three planes: the coronal plane passing through the PC, the midsagittal plane, and axial plane passing through the highest, most superior (most dorsal) point of the parietal cortex.

I: The point of intersection of three planes: the coronal plane passing through the PC, the midsagittal plane, and axial plane passing through the lowest, most inferior (most ventral) point of the temporal cortex.

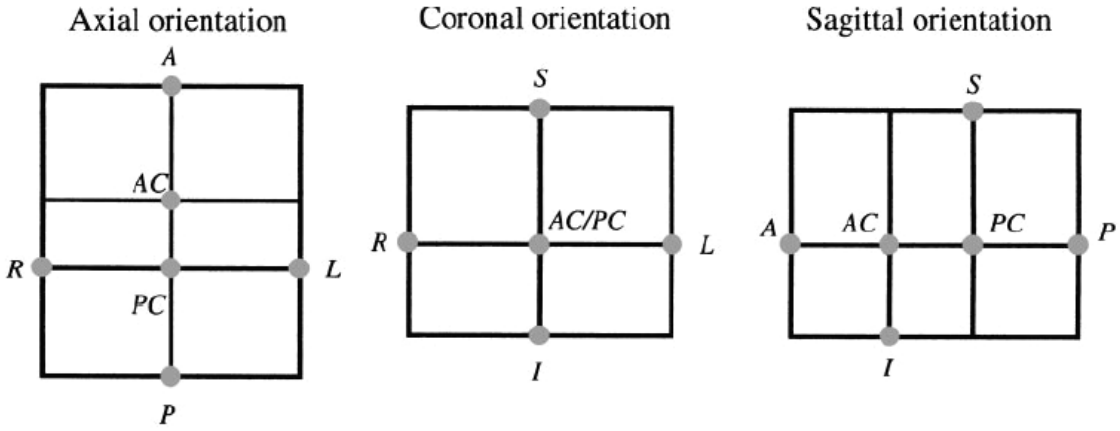

Figure 15 Modified Talairach Landmarks

For our project, we need the information of the modified Landmarks in the electronic slice. The modified Talairach landmarks coordinate in electronic slices are in *Fig.* 16 The coordinate is (row, column) in pixel.

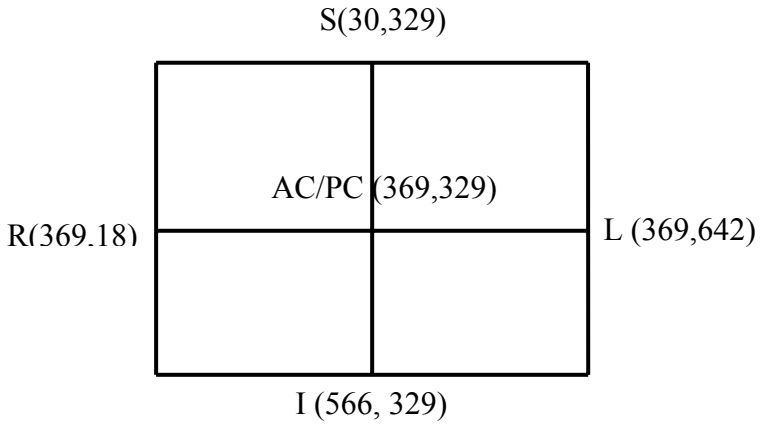

Figure 16 The modified Talairach landmarks coordinate in coronal direction

4.2 Local segmentation

After finding the coarse position of the object, the local segmentation step is to identify the exact boundary of the object. This is the refinement of the coarse

boundary of hippocampus after global segmentation. An active contour is applied to segment the exact boundary of the structure. We have explored some models of active contour in this study.

In *Fig.* 17 we describe the detailed steps of local segmentation. First, the 3D image ".raw" file is input and stored in a 3D matrix for further implementation. Each image slice is represented by a 2D array from this 3D matrix. Based on the modified Talairach landmarks, the region of interest (ROI) is extracted. The Canny edge detector is applied in the ROI to find its edge map. The anatomical constraint is put into the edge map. The atlas slice ".bmp" files are input and stored in a 2D array when running a 2D image slice. The ROI in the atlas slice is extracted based on the modified Talairach landmarks as well. From the atlas ROI, the atlas boundary of hippocampus is searched based on the color code and is matched into the image ROI as initialization of the active contour. The edge map is the input for GVF and the active contour runs on this GVF to converge to the exact boundary of the hippocampus.

The details what we have implemented are explained below.

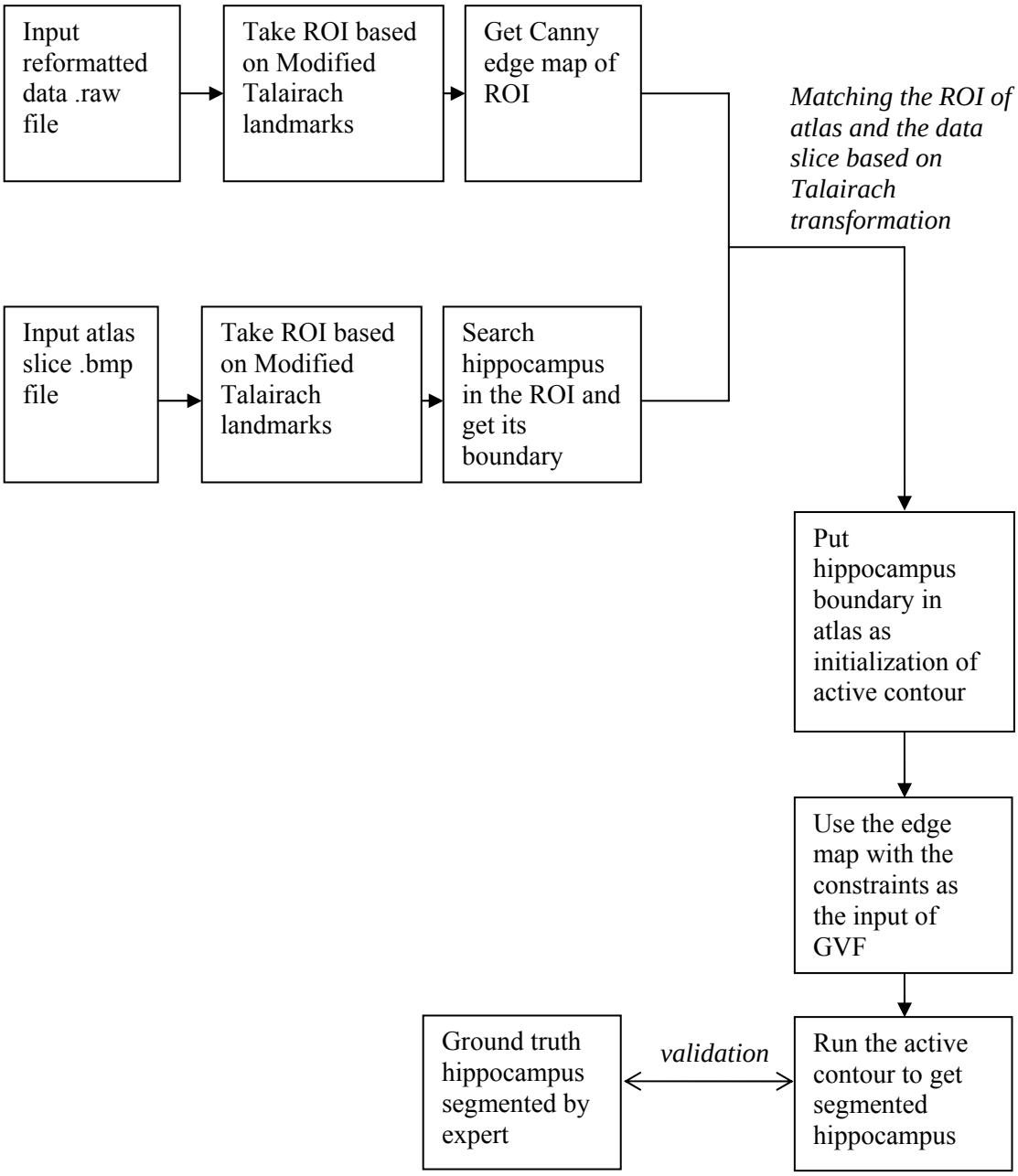

Figure 17 Flowchart describing atlas-assisted local segmentation.

From the image slice, we get the region of interest based on the modified Talairach landmarks. The co-ordinate values of the modified Talairach landmarks

are obtained from the global segmentation. The left hippocampus is the object to be segmented. (See *Fig.* 18). The ROI is extracted using the coordinates of the landmarks AC, R and I.

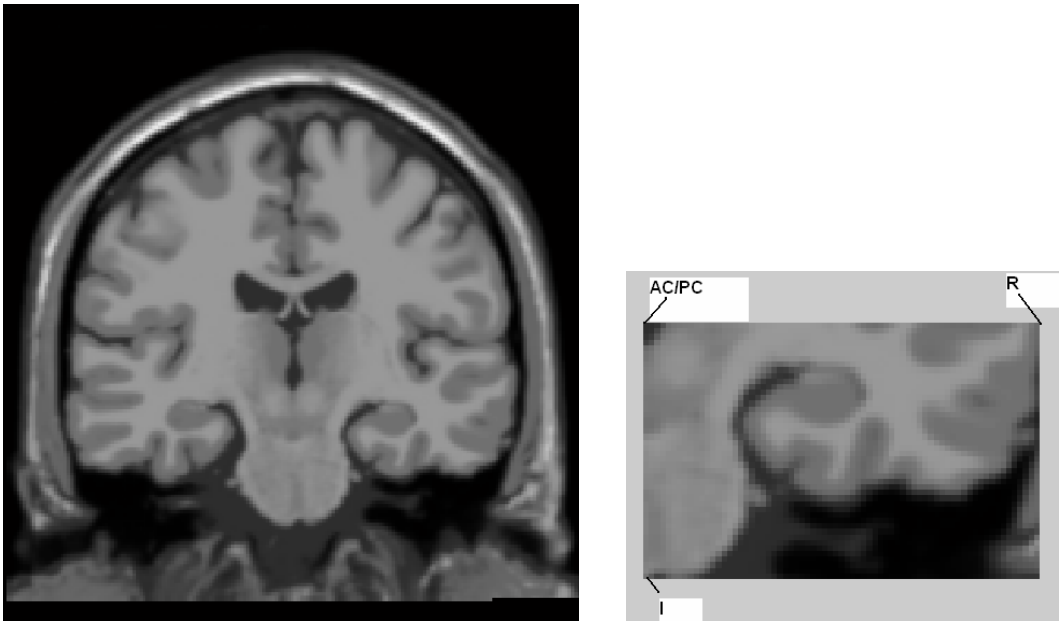

Figure 18 One data image slice and its corresponding ROI.

From the atlas slice, we also get the region of interest based on the modified Talairach landmarks. The region of interested is defined like in the *Fig* 19.

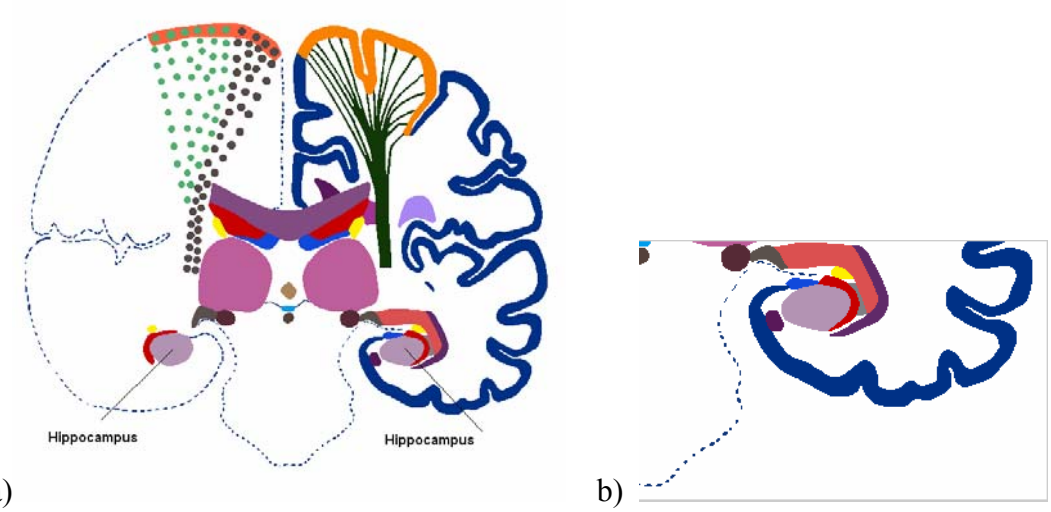

a) b)

Figure 19 The region of interest based on the modified Talairach landmarks. a) The atlas b) The region of interest.

The atlas plates are color-coded. Therefore, to find the hippocampus in the atlas, the color value of the hippocampus is searched. This value is different from other structures in the atlas. The color code of hippocampus is [179 147 179] in the range from 1 to 255. After finding the hippocampus, we mark the atlas only with the hippocampus in white (1 value) and the rest in black (0 value). Running the "edge" function in Matlab, we get the contour that covers the hippocampus. This contour is our initialization for the active contour. The initial points of the active contour are stored in two array *x* (row co-ordinate) and *y* (column co-ordinate). The length of these two arrays depends on the number of points of the active contour. The lengths as well as the values of these two arrays are updated when the active contour runs iteratively.

Figure 20 After finding the hippocampus in the atlas

a) 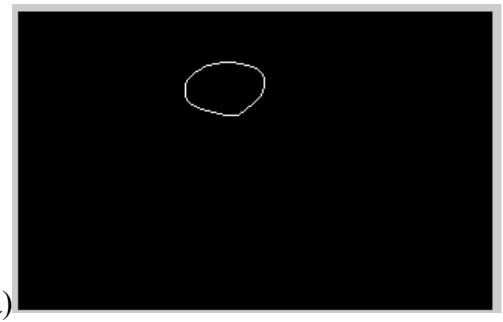 b) 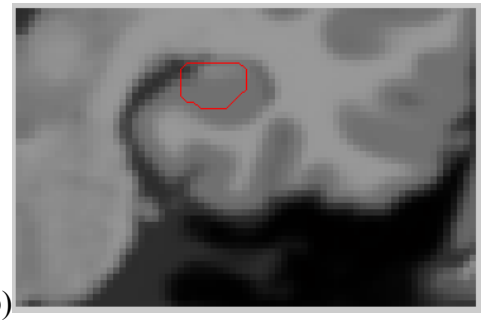

Figure 21 The edge of the hippocampus from the atlas is detected (Fig a)) put as the initialization of the active contour (Fig b))

Match the atlas with the image slice

For initialization of the active contour, we match the boundary of hippocampus from the atlas as the initialization of the active contour to its corresponding image slice. In the Table 1, there are some image slices and their corresponding atlas slices.

Coronal Direction Image Slice	Atlas Slices
TT88c / 0mm	#16 (the slice that contains AC)
TT88c / -4mm	#17
TT88c / -8mm	#18
TT88c / -12mm	#19
TT88c / -16mm	#20
TT88c / -20mm	#21
TT88c / -24mm	#22
TT88c / -28mm	#23
TT88c / -32mm	#24
TT88c / -35mm	#25
TT88c / -40mm	#26

Table 1 The data image slices and its corresponding atlas plates.

In the left column in Table 1, there are coronal direction image slices. The 0mm slice is the one that contains the AC landmarks. In the right column, there are corresponding atlas slices with the image slices in the left. There are 38 atlas

slices in the coronal direction. Hippocampus appears in the atlas slices numbered from 19 to 26. In the table, the minus slice means that it is near posterior.

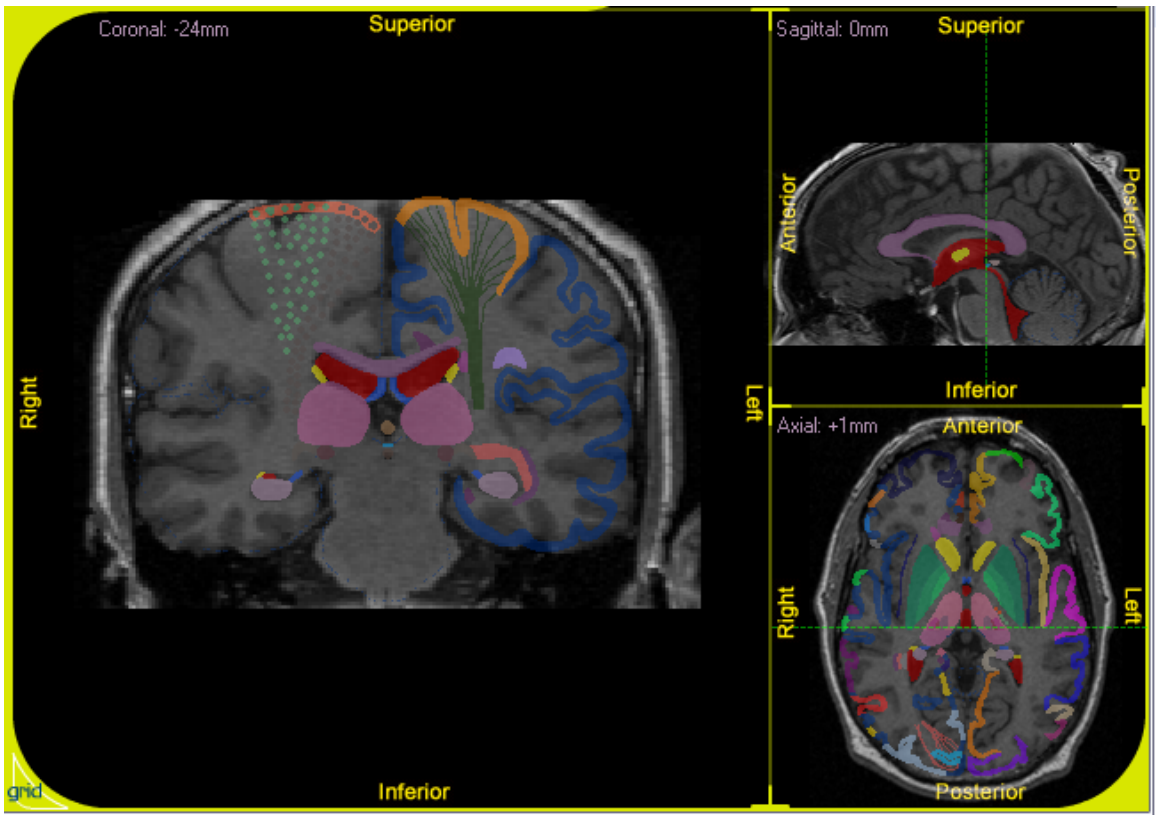

Figure 22 An illustration of a coronal atlas slice at the co-ordinate -24mm, and corresponding position of this slice in the sagittal and axial direction (green line).

Canny edge map

To make the active contour converge easily, an edge map of the region of interest is computed. From experiments, we found that the Canny edge detector gives a good edge map. (See *Fig.* 23).

a)  b) 

Figure 23 The region of interest and the corresponding Canny edge map.

Apply anatomical knowledge to active contour

To make the active contour converge more precisely, the size and shape of hippocampus is converted to constraint of the active contour. To put the prior anatomical information, we use the atlas boundary into the edge map. The value of all pixels in the Canny edge is 0 or 1 (0 is normal pixel and 1 is in the edge). Therefore, we set value α corresponding to the atlas boundary in the range [0..1]. The higher the value of α is, the more difficult for the active contour to move far away from the atlas boundary. In *Fig*. 24 the edge in gray color is the anatomical constraint edge as well as the initialization boundary active contour.

Figure 24 The edge map with the constraint of the atlas boundary.

Running the active contour

Before choosing GVF as a choice for the running of active contour, experiments with traditional snake were tried. Moreover, I also had tried the GVF with the input as the gradient map of the image. I found that the GVF with the edge map input gave a good accuracy of boundary as well as a high speed convergence.

The modified edge map with constraint is blurred by applying Gaussian noise function (see *Fig*. 25). The blurred edge map is used as input for the calculation of GVF. After each iteration, the contour is interpolated to make sure it is smooth enough for the next running time. The iterative procedure of snake deformation is run for a fixed number of iterations (100 times).

Figure 25 The edge map after applying the Gaussian noise function.

Filling the final active contour

After running the algorithm of the active contour, we just get the boundary of the structure. From the center of the active contour, we grow the seed in this center to get the segmented region. The region growing algorithm is applied to fill up the region inside the active contour (See *Fig.* 26).

Fill_contour algorithm: from the contour we find the center of the contour. The center is found by the mean of all the points of the contour. The center of the manual segmentation is also found by calculating the mean of all the points marked by the experts. After finding the center, we run the Region_Growing algorithm to fill up the region inside the boundary.

Region_growing: the input of the algorithm is the matrix that contains the contour and the center that we want to grow to get the region, and the value of the boundary and the value that we want to fill up the region.

a) 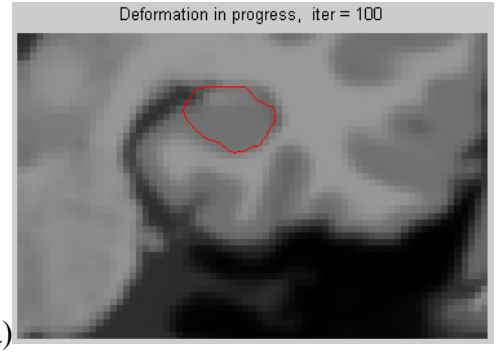

b) 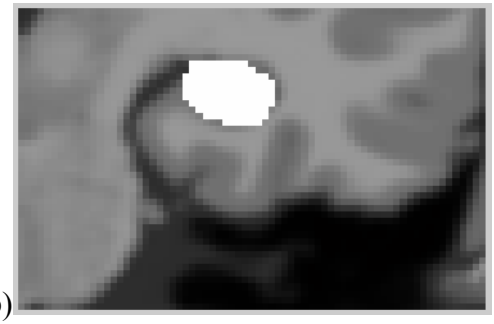

Figure 26 The hippocampus segmented with the final active contour and filled to form a segmented region

Chapter 5

Results and Validation

Validation

In order to quatitatively evaluate the algorithm, 10 data sets have been selected. Hippocampus was also segmented manually by an expert. The manual segmentation of the experts is the ground truth for validation of the algorithm.

The overlap metric [Zidenbos 1994] was calculated to compare the hippocampus manually and automatically segmented:

$$\varepsilon = 2 \times V_{12} /(V_1 + V_2)$$

where V_1 and V_2 are the volumes of the two segmentations, and V_{12} is the volume of their overlap. In addition, the ratios of the volume of false negative (missed) and false positive (overestimated) to the overlap volume are computed (in percentage). False negative (FN) is defined as the yellow region in *Fig*. 27. This yellow is extracted by the expert, but not by the algorithm (missed). False positive (FP) is defined as the red region in the *Fig.* 27. This red region is extracted by the algorithm but not by the expert (overestimated).

FN ratio = (number of pixels in yellow region)/ (number of pixels in green region)

FP ratio = (number of pixels in red region)/ (number of pixels in green region)

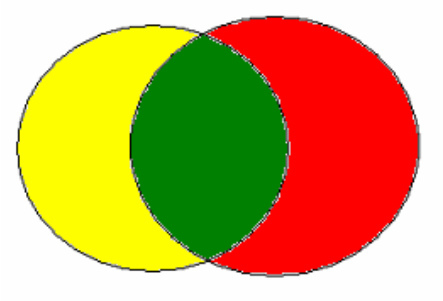

Figure 27 Definition of false negative (yellow) and false positive (red).

The final results of 10 data sets are in the table 2.

Data	Overlap metric	False Negative Ratio	False Positive Ratio
BrainWeb 1100	0.94	2%	9.6%
Child 02	0.94	1.8%	10%
IB 0610	0.935	2%	11%
IB 1103	0.91	8%	10%
Japan 07	0.92	4%	12%
Japan 13	0.91	8%	12%
Japan 14	0.94	2%	10%
Singapore 07	0.91	8%	11%
Singapore 13	0.9	2%	18%
Singapore 18	0.9	1.8%	19%
Average	0.9205	3.88%	12.26%

Table 2 The hippocampus segmentation results of 10 data sets

We present some good examples as well as some issues of the algorithm and outstanding comments below.

From *Fig.* 28 to *Fig.* 34, there are some results.

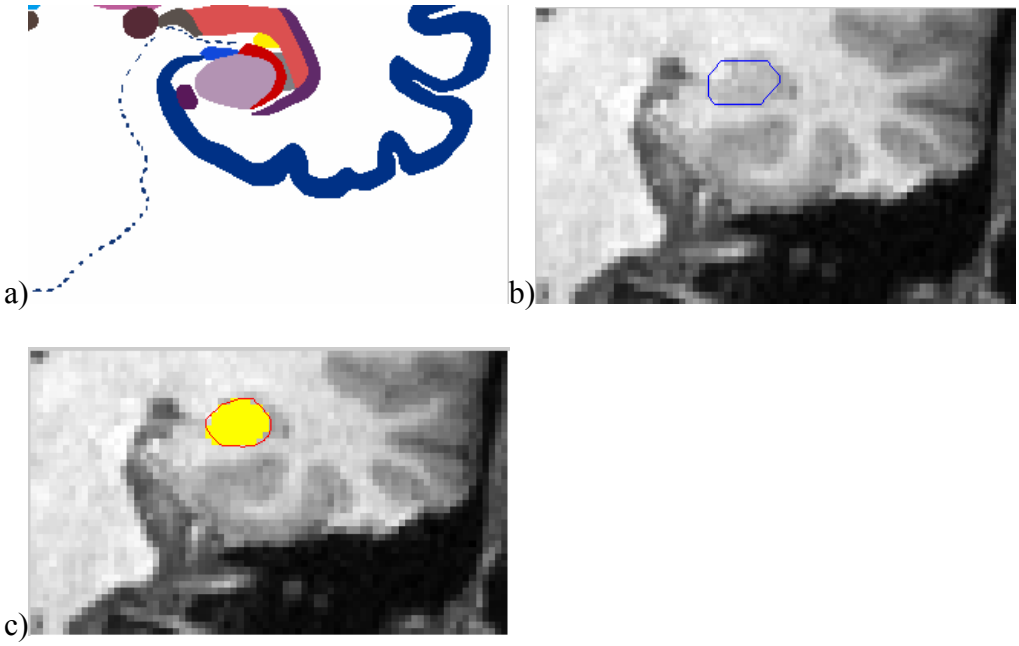

Figure 28 Child02 Image slice number = 125; Atlas slice number = 22; α = 0.7 a) The atlas b)The initial boundary c) The final boundary and the ground truth in yellow.

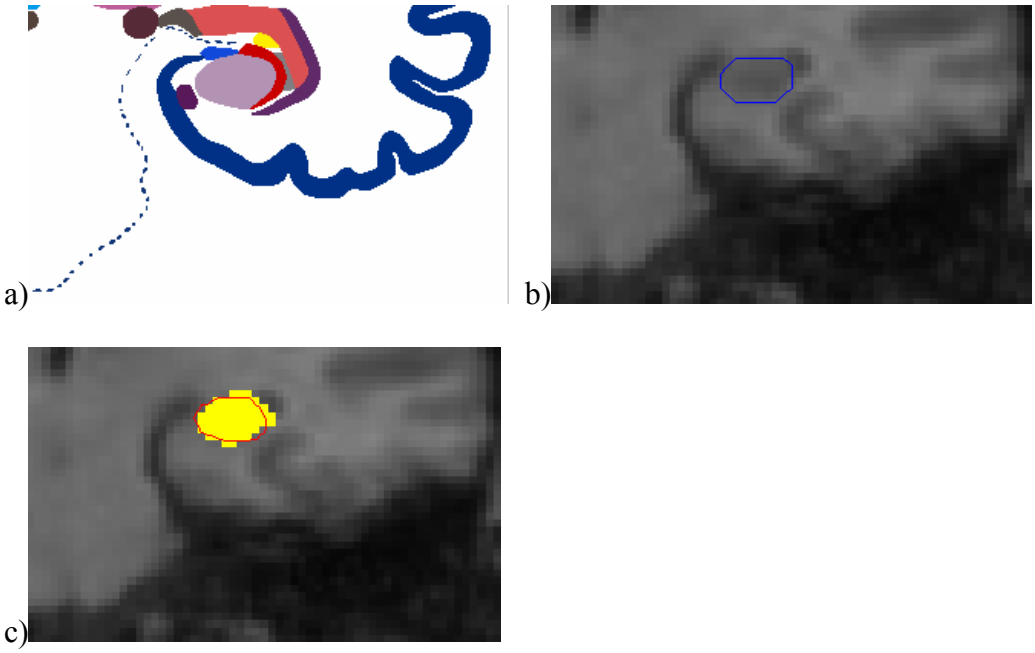

Figure 29 Ib0610 Image slice number = 110; Atlas slice number = 22; α = 0.7 a) The atlas b)The initial boundary c) The final boundary and the ground truth in yellow.

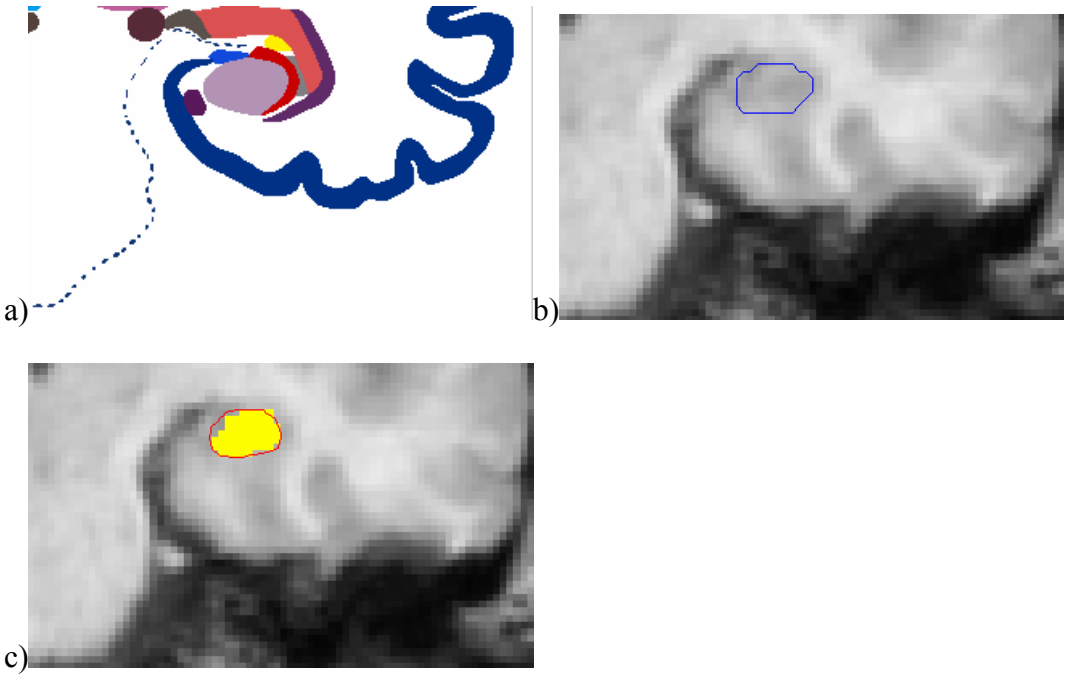

Figure 30 Ib1103 Image slice number = 116; Atlas slice number = 22; α = 0.7 a) The atlas b) The initial boundary c) The final boundary and the ground truth in yellow.

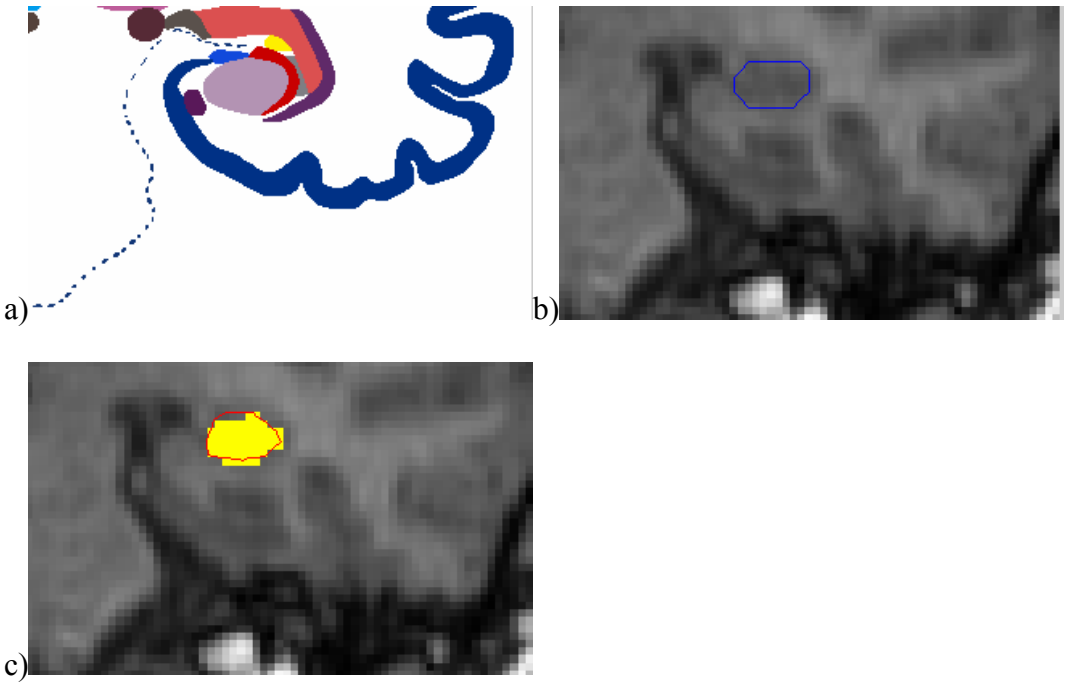

Figure 31 Ja07Image slice number = 150; Atlas slice number = 22; α = 0.7 a) The atlas b) The initial boundary c) The final boundary and the ground truth in yellow.

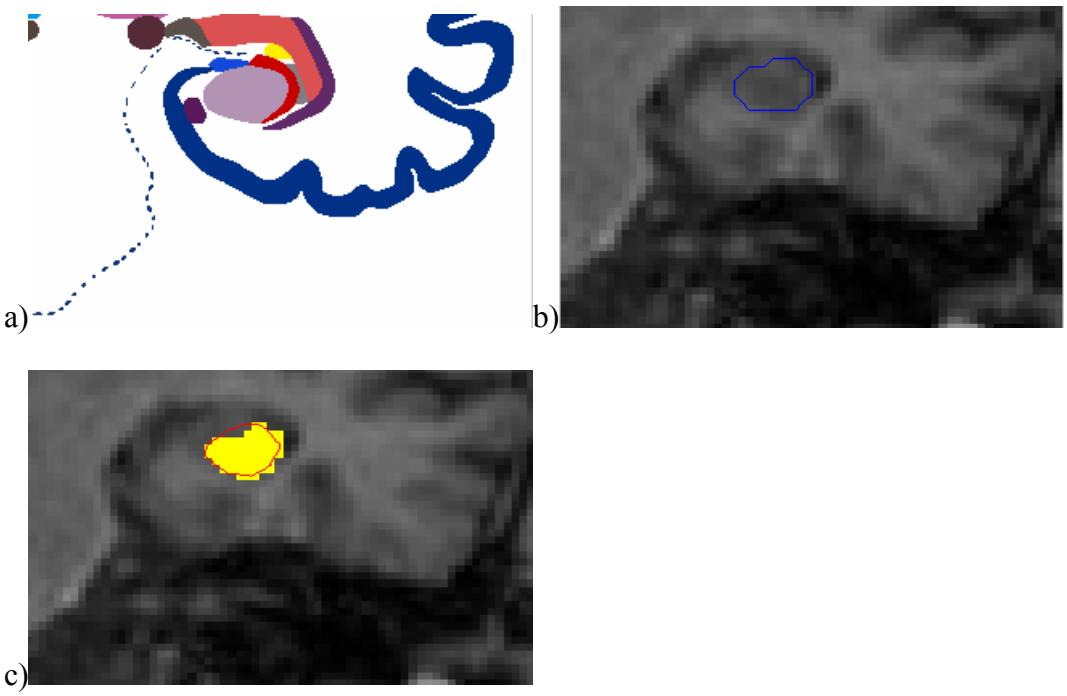

Figure 32 Image slice number = 172; Atlas slice number = 22; α = 0.7 a) The atlas b)The initial boundary c) The final boundary and the ground truth in yellow.

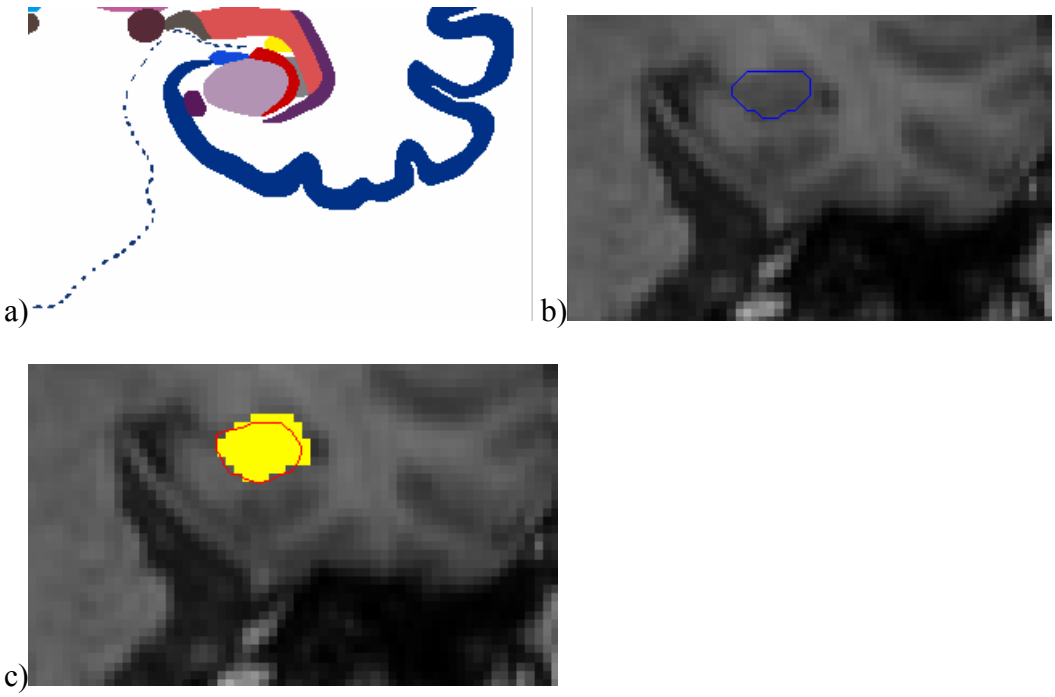

Figure 33 Ja14 Image slice number = 137; Atlas slice number = 22; α = 0.7 a) The atlas b)The initial boundary c) The final boundary and the ground truth in yellow.

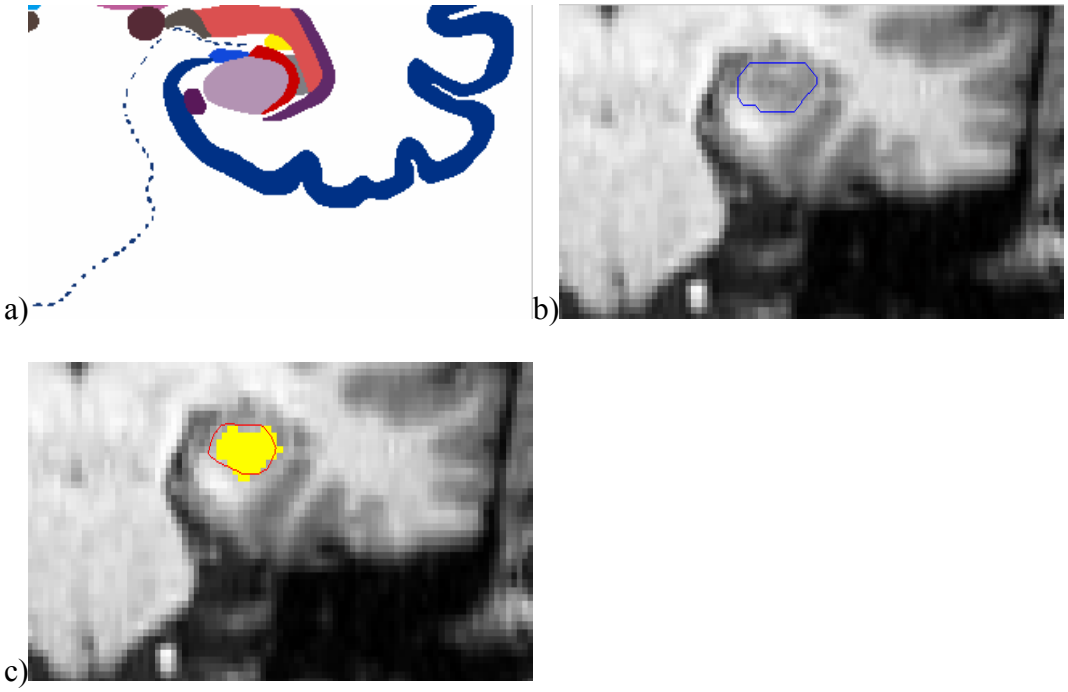

Figure 34 Sg18 Image slice number = 143; Atlas slice number = 22; α = 0.7 a) The atlas b)The initial boundary c) The final boundary and the ground truth in yellow.

In some data, the false negative ratio is so high than others. This is because the active contour does not cover all the hippocampus (missed) (See *Fig.* 35).

a)  b) 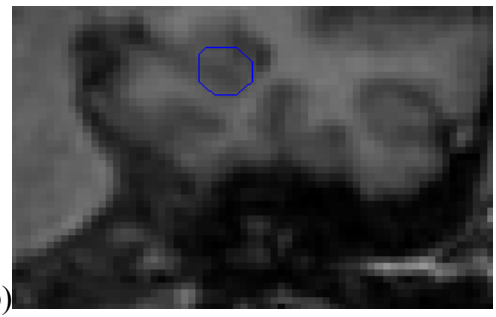

c) 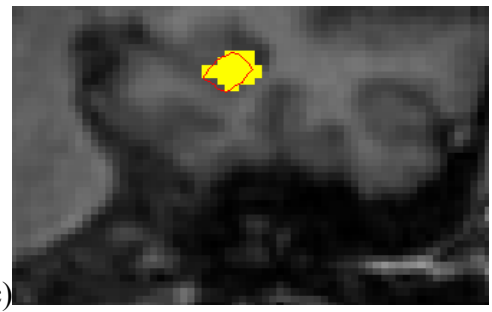

Figure 35 Ja13 Image slice number = 172; Atlas slice number = 23; α = 0.6 a) The atlas b)The initial boundary c) The final boundary and the ground truth in yellow.

From the result table, we see that the false positive ratio is mostly higher than the false negative ratio. Because the active contour usually is slightly pulled by the nearest edges, it overextracts the hippocampus (See *Fig.* 36, *Fig.* 37).

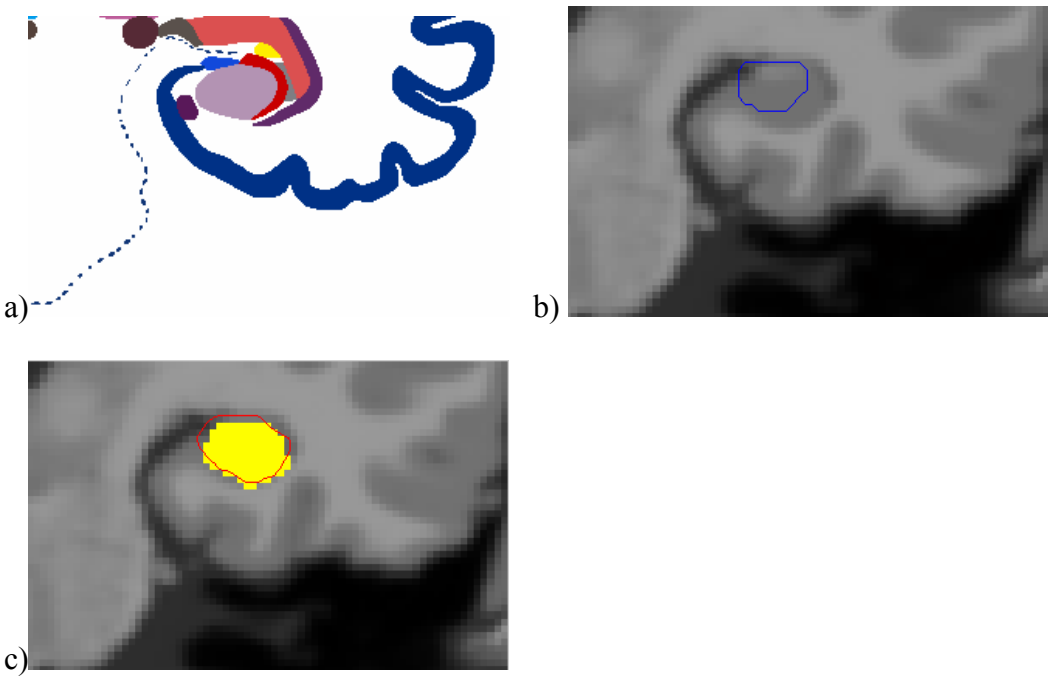

Figure 36 BW1100 Image slice number = 117; Atlas slice number = 22; α = 0.7 a) The atlas b)The initial boundary c) The final boundary and the ground truth in yellow.

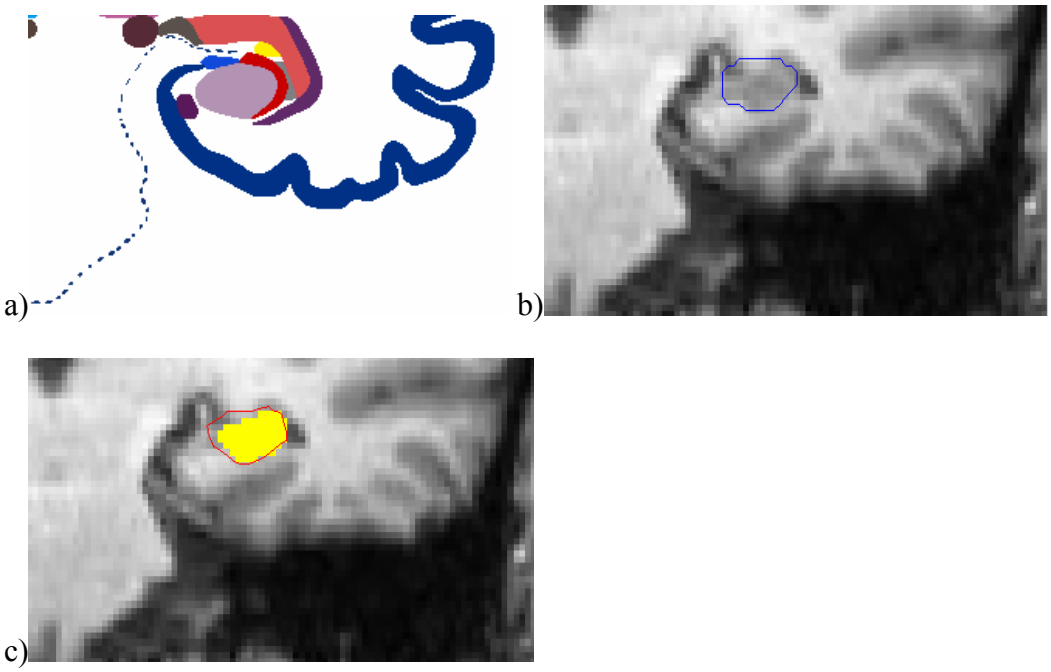

Figure 37 Sg13 Image slice number = 150; Atlas slice number = 22; α = 0.7 a) The atlas b)The initial boundary c) The final boundary and the ground truth in yellow.

In some slices, when the edge map is not sufficient and the initialization is not so exact, it is difficult for the active contour to run. In this case, if we set the constraint value α be so high (for example greater than 0.8), the active contour is not so accurate because it can not apply much information in the image. It just converges well because of the prior constraint. However, this is a solution to segment hippocampus in slices where there is much noise and no edge around detected. If the edge can not be detected, the constraint becomes a very important knowledge to segment the hippocampus (see *Fig.* 38).

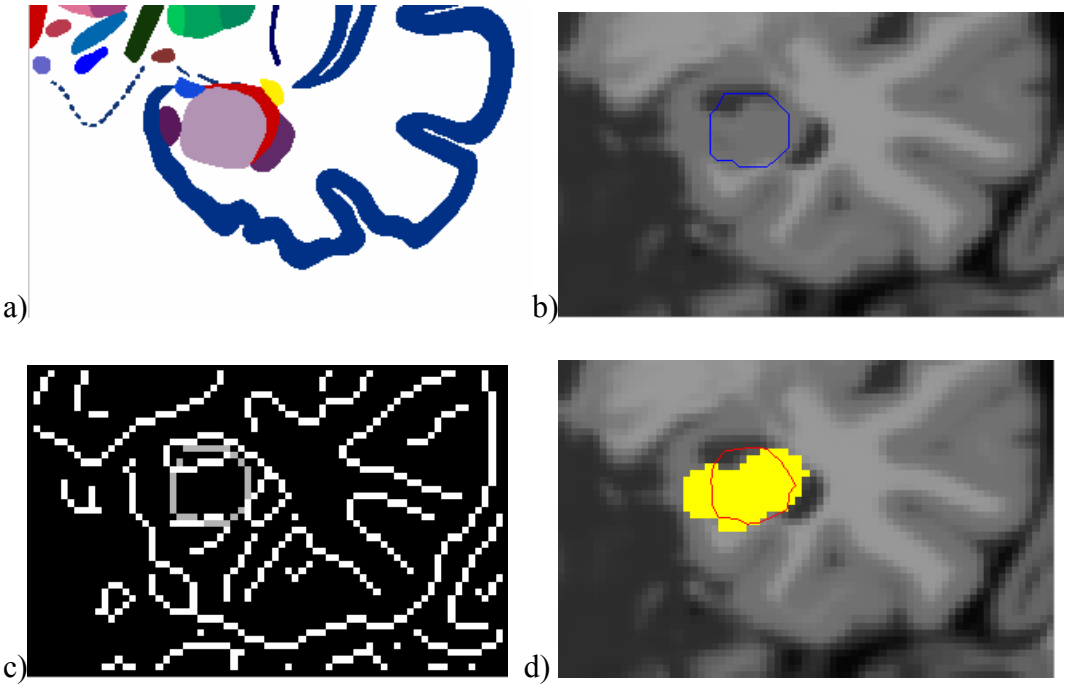

Figure 38 Image slice number = 105; Atlas slice number = 19; α = 0.7 a) The atlas b)The initial boundary c) The edge with constraint d) The final boundary and the ground truth in yellow.

In some cases, there is noise in the image. An edge appears inside the region of the actual hippocampus. When the active contour runs, it converges to wrong inside edge instead of the exact boundary edge. (See *Fig.* 39).

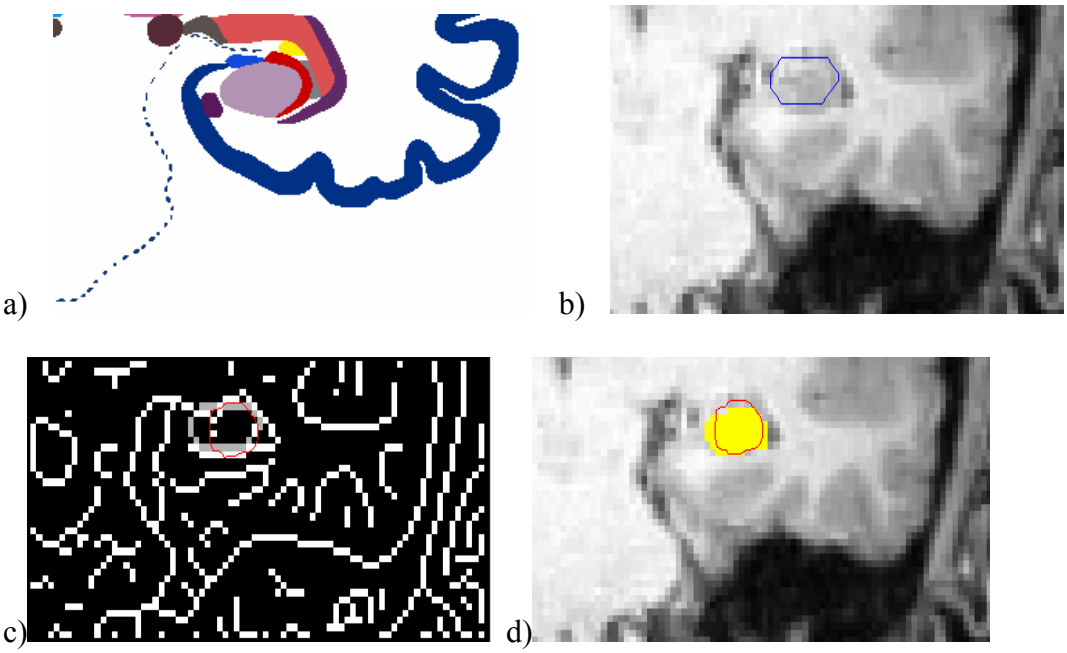

Figure 39 An example of the active contour converging an noise edge.

One solution in this case is to increase the value of α. This means that we make the constraint become stronger, so the active contour can not go far away from the initialization and converge to a wrong edge. (See *Fig* . 40)

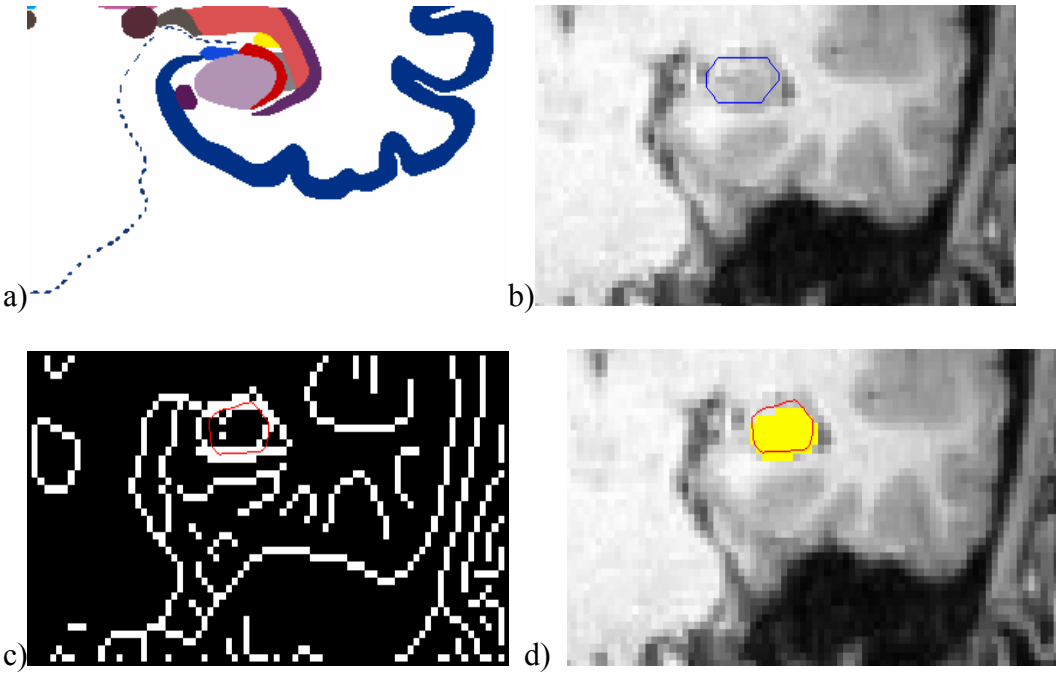

Figure 40 An example of reducing the influence of noise edge by increasing the constraint value α (In this example α =1).

Chapter 6

Conclusion and Prospects

Advantages

- Our algorithm is fully automatic and no manual intervention is required.
- The approach combines the anatomical knowledge with image processing technique.
- The algorithm can also be applied for other structures of brain image.

As the algorithm is based on the combination of image processing technique and anatomical knowledge, it may well be extended to other imaging sequences and other modalities.

Limitation

The algorithm should be improved to increase the accuracy. The average value of the metric is 0.9205. That is not a high value for a segmentation algorithm. More information in the image should be added as the constraint of the active contour to get better accuracy of segmentation. More detailed information about the shape and the texture of the anatomic structure of interest could be transferred to the model by applying the methods similar to those described in our approach.

Controlling the running of the active contour is not an easy task. For the edge-based active contour, the appearance of some noise edge decreases the accuracy of

the segmentation. The edges of the nearby objects also influence the accuracy of the algorithm.

Conclusion

In this thesis, we have presented an atlas-assisted active contour to segment hippocampus. The purpose of this work is mainly to identify hippocampus location and segment quickly. To overcome some obstacles of the traditional active contour, we use anatomical information as constraints to the active contour. Therefore, the active contour can more easily converge to the desired boundary of the hippocampus.

Fast and accurate segmentation of brain structures from MRI is a difficult task due to several factors, including anatomical variability, diversity of pulse sequences, various scanners, noise, partial volume effect, intensity inhomogeneity, artifacts, just to mention a few. Atlas-based segmentation helps in fast brain segmentation. In our work, we have used our electronic version of the Talairach-Tournoux brain atlas with gross anatomy in coronal orientations to demonstrate the atlas and snakes based segmentation. The GVF snake gives a good result when the edge map can be derived. The anatomical knowledge of hippocampus is put into the algorithm to make the active contour converge more easily. Although applying active contour is not completely satisfactory, the problem can be improved by adding more techniques of medical image segmentation.

Prospects

Our algorithm provides a good approach in automatically identifying and segmenting hippocampus from MR images. There are still some space work left to be done in the future.

Our future work is to improve our algorithm so that it can run well in slices where hippocampus and amygdala are overlapped. Our approach also should be experimented in many more data sets with different modalities and contrast and some more active contours. The matching from electronic atlas is another issue to improve in future work. If the matching is precise, the initial boundary of the active contour is closer to the actual boundary of the structures. In that case, we can have an initial constraint that the snake can not move so far from the initial boundary. The results are encouraging. However, more work is required to address problems existing in clinical setting.

One prospect of segmentation of hippocampus is statistical shape analysis (SSA) of hippocampus. SSA has become of increasing interest to the neuroimaging community due to its potential to precisely locate morphological changes and thus potentially discriminate between healthy and pathological structures. SSA is frequently used method to address the problem of shape variation. These methods try to find the statistical property of the variation in a population. The result of SSA can be used to construct the probabilistic atlas. See (*Fig.* 41).

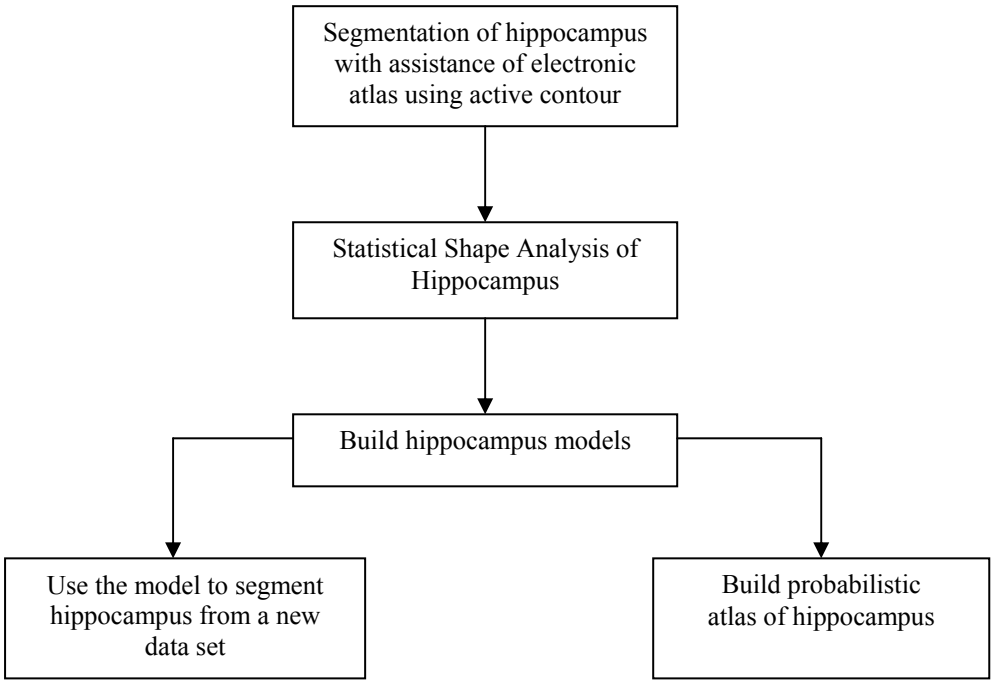

Figure 41 Next prospective steps of segmentation of hippocampus

Author's Publication

1. Pham Duc Minh, K. N. Bhanu Prakash and W.L. Nowinski, "Brain Atlas-assisted Segmentation of the Hippocampus from MR Neuroimages", *1st International Bioengineering Conference 2004 (IBEC 2004).*

References

[Ahmed] Mohamed N. Ahmed, "Novel image segmentation and registration algorithms for the study of brain structure and function", PhD Thesis, University of Louisville, Louisville, Kentucky

[Ashton 1997] A. Ashton, J. Parker, J. Berg, Chang Wen Chen, "Novel volumetric feature extraction technique with applications to MR images", *IEEE Transaction on Medical Imaging*, 16(4): 365-371, Aug. 1997.

[Barra 2001] Vincent Barra and Jean-Yves Boire, "Automatic segmentation of subcortical brain structures in MR Images using information fusion", *IEEE Transactions on Medical Imaging*, Vol. 20, No. 7, July 2001.

[Cohen 1991] L. D. Cohen, "On active contour models and balloons", *CVGIP: Image Understanding*, 53(2):211-218, 1991

[Cohen 1993] L. D. Cohen and I. Cohen, "Finite-element methods for active contour models and balloons for 2-D and 3-D images", IEEE Trans. Pattern Anal. Machine Intell., vol. 15, pp. 1131-1147, Nov. 1993.

[Crum 2001] W. R. Crum, R. I. Schill, and Nick C. Fox, "Automated hippocampus segmentation by regional fluid registration of serial MRI: validation and application in Alzheimer's disease", NeuroImage, 13, 847-855, 2001.

[Csernansky 1998] J.G. Csernansky, S. Joshi, L. Wang, J.W. Haller, M. Gado, J.P. Miller, U. Grenander, M.I. Miller. "Hippocampal morphometry in schizophrenia by high dimensional brain mapping". *Proc. Natl. Acad.Sci. USA*, 95 (19): 11406-11411 SEP 15 1998.

[Dzung 1998] Dzung L.Pham, Chenyang Xu, Jerry L. Prince, "A survey of current

methods in medical image segmentation", Annual Review of Biomedical Engineering, January 19, 1998.

[Dzung 1999] Dzung L. Pham, and Jerry L. Prince, "Adaptive Fuzzy Segmentation of Magnetic Resonance Images", *IEEE Transactions on Medical Imaging*, Vol. 18, No. 9, September 1999.

[Geraud 1998] T. Geraud, I. Bloch, H. Maitre, "3D Segmentation of Brain Structures from MR Images using Morphological Approaches", Medical Image Analysis.

[Ghanei 1998] A. Ghanei, H. Soltanian-Zadeh, J.P. Windham. "A 3D deformable surface model for segmentation of objects from volumetric data in medical images", *Computers in Biology and Medicine*, 28(3):239-253, May 1998.

[Haller 1997] J.W. Haller, A. Banerjee, G.E. Christensen, M. Gado, S. Joshi, M.I. Miller, Y. Sheline, M.W. Vannier, J.G. Csernansky, "Three-dimensional hippocampal MR morphometry with high-dimensional transformation of a neuroanatomic atlas", *Radiology*, 202 (2): 504-510, FEB 1997.

[Hu 2003] Q. Hu and W. L. Nowinski, "A rapid algorithm for robust and automatic extraction of the midsagittal plane of the human cerebrum from neuroimages based on local symmetry and outlier removal", NeuroImage 20(2003) 2153-2165.

[Hult 2003] Roger Hult, "Segmentation and Visualization of Human Brain Structures", PhD Thesis, Uppsala University 2003.

[Joshi 1997] S. C Joshi, M. I Miller, U. Grenander, "On the geometry and shape of brain submanifolds", International Journal of Pattern Recognition and Artificial Intelligence, 11:1317-1343, 1997.

[Kang 2003] Y. Kang, K. Engelke, and A. Kalender, "A new accurate and precise 3-D segmentation method for skeletal structures in volumetric CT data", *IEEE Trans. Med. Imag*., vol. 22, no. 5, may 2003, pp. 586-598.

[Karayiannis 1999] N. B. Karayiannis and Pin-I Pai, "Segmentation of Magnetic Resonance Images using fuzzy algorithms for Learning Vector Quantization", *IEEE Transactions on Medical Imaging*, Vol. 18, No. 2, February 1999.

[Kass 1987] M. Kass, A. Witkin and D.Terzopoulos, "Snakes: Active contour models", *Int. Journal of Computer Vision*, 1:321-331, 1987.

[Klemen 1999] A. Kelemen, G. Szekely, and G. Gerig. "Elastic model-based segmentation of 3-D neuroradiological data sets". *IEEE Transactions on Medical Imaging*, 18(10): 828-839, October 1999.

[McInerney 1996] T. McInerney, and D. Terzopoulos, "Deformable Models in Medical Image Analyis: A Survey", *Medical Image Analysis*, 1(2):91-108, 1996.

[Nowinski 1997a] Nowinski WL, Bryan RN, Raghavan R, "The electronic clinical brain atlas. Multiplanar navigation of the human brain", Thieme, New York, Stuttgart

[Nowinski 1997b] Nowinski WL, Fang A, Nguyen BT, "Multiple brain atlas database and atlas-based neuroimaging system". Comput Aided Surg 2:42–66

[Nowinski 2000]Nowinski WL, Yang GL, Yeo TT, "Computer-aided stereotactic functional neurosurgery enhanced by the use of the multiple brain atlas database", IEEE Transactions on Medical Imaging 2000;19(1):62-69.

[Nowinski 2001]Nowinski WL, Thirunavuukarasuu A (2001b), "Atlas-assisted localization analysis of functional images", Medical Image Analysis 2001;5(3):207-220.

[Nowinski 2001a] W.L. Nowinski, "Modified Talairach Landmarks", *Acta Neurochirurgica*, 143(10), 1045-1057, 2001.

[Nowinski 2001c] Nowinski WL, "Computerized brain atlases for surgery of movement disorders", Semin Neurosurg 12:183–194

[Nowinski 2002] Nowinski WL, "Electronic Brain Atlases: Features and Applications" in "3D Image Processing: Techniques and Clinical Applications", Medical Radiology series, Springer-Verlag, 2002.

[Nowinski 2003a] Nowinski WL, Belov D, **"**The Cerefy Neuroradiology Atlas: A Talairach-Tournoux atlas-based tool for analysis of neuroimages" Neuroimage. 2003 Sep;20(1):50-7.

[Pham 2004] Pham Duc Minh, K. N. Bhanu Prakash and W.L. Nowinski, "Brain Atlas-assisted Segmentation of the Hippocampus from MR Neuroimages", *1st International Bioengineering Conference 2004 (IBEC 2004).*

[Reyes-Aldasoro 1999] Constantino Carlos Reyes-Aldasoro, "Image Segmentation with Kohonen Neural Network Self-Organising Maps", 1999.

[Rohlfing 2004] T. Rohlfing, D. B. Russakoff and C. R. Maurer, "Performance-based classifier combination in Atlas-based image segmentation using expectation-maximization parameter estimation", *IEEE Transactions on Medical Imaging*, Vol. 23 , No. 8, August 2004, Pages:983 - 994.

[Shen 2001a] D. Shen, E. H. Herskovits and C. Davatzikos, "An adaptive-focus statistical shape model for segmentation and shape modeling of 3-D brain structures", *IEEE Transactions on Medical Imaging*, Vol. 20 , No. 4, April 2001.

[Shiffan 2000] S. Shiffman, G. D. Rubin, and S. Napel, "Medical Image segmentation using analysis of isolable-contour maps", *IEEE Transactions on Medical Imaging*, Vol. 19, No. 11, November 2000.

[Staib 1992] Lawrence H. Staib, and James S. Duncan, "Boundary Finding with Parametrically Deformable Models", IEEE Transaction on Pattern Analysis and Machine Intelligence, Vol. 14, No. 11, November 1992, Pages 1061:1075.

[Szekely 1996] Gabor Szekely, A. Kelemen, C. Brechbuhler and G. Gerig, "Segmentation of 2-D and 3-D objects from MRI volume data using constrained

elastic deformations of flexible Fourier contour and surface models", Medical Image Analysis (1996), Volume 1, number 1, pp 19-34.

[Xu 1998] C. Xu and J. L. Prince, "Snakes, Shapes, and Gradient Vector Flow", *IEEE Transactions on Image Processing*, 7(3):359-369, 1998.

[Zidenbos 1994] Zidenbos, A.P. , Dawant, B.M. , Margolin, R.A., Palmer, A.C., 1994. Morphometric analysis of white matter lesion in MR images: method and validation, *IEEE Transactions on Medical Imaging*, 13, 716-724.